Contribution of recycled moisture to local precipitation in the inland Heihe River Basin

Liangju Zhao[a, b,*], Xiaohong Liu[c], Ninglian Wang[a], Yanlong Kong[d], Yaoxuan Song[b], Zhibin He[b], Quanyu Liu[a], Lixin Wang[e,*]

[a] Shaanxi Key Laboratory of Earth Surface System and Environmental Carrying Capacity, College of Urban and Environmental Sciences, Northwest University, Xi'an 710127, China

[b] Key Laboratory of Ecohydrology and Integrated River Basin Science, Northwest Institute of Eco-Environment and Resources, Chinese Academy of Sciences, Lanzhou 730000, China

[c] School of Geography and Tourism, Shaanxi Normal University, Xi'an 710119, China

[d] Key Laboratory of Engineering Geomechanics, Institute of Geology and Geophysics, Chinese Academy of Sciences, Beijing, China

[e] Department of Earth Sciences, Indiana University-Purdue University Indianapolis (IUPUI), Indianapolis, IN 46202, USA

Running title: Contribution of recycled moisture to precipitation

***Corresponding author**

Dr. Liangju Zhao

College of Urban and Environmental Sciences

Northwest University

Xi'an, Shaanxi, 710069, China

E-mail: zhlj@nwu.edu.cn; Cell phone：15934832330

Dr. Lixin Wang

Department of Earth Sciences

Indiana University-Purdue University Indianapolis

Indianapolis, IN, 46202, USA

E-mail: lxwang@iupui.edu; Office phone number: 317-274-7764

This is the author's manuscript of the article published in final edited form as:

Zhao, L., Liu, X., Wang, N., Kong, Y., Song, Y., He, Z., … Wang, L. (2019). Contribution of recycled moisture to local precipitation in the inland Heihe River Basin. Agricultural and Forest Meteorology, 271, 316–335. https://doi.org/10.1016/j.agrformet.2019.03.014

ABSTRACT

Recycled moisture contributed by continental evaporation and transpiration plays an important role in regulating the hydrological processes and atmospheric humidity budget in arid inland river basins. However, knowledge of moisture recycling within many large inland basins and the factors that control moisture recycling is generally lacking. Based on a three-component isotopic mixing model, we assessed the characteristics of moisture recycling in China's semi-arid Heihe River Basin. During the active growing season, almost half of the precipitation in the upper reaches was provided by local moisture recycling, and the main contribution came from transpiration. In the middle reaches, almost half of the precipitation in the artificial oasis and the desert-oasis ecotone was also provided by local moisture recycling, and the transpiration fraction (f_{Tr}) and evaporation fraction (f_{Ev}) of the artificial oasis differed from those of the desert-oasis ecotone. In the lower reaches, less than 25% of the precipitation was provided by local moisture recycling. Mean f_{Tr} values were relatively low in the Gobi (15.0%) in the middle reaches and in the riparian forest at Ejina (25.6%) in the lower reaches. The positive correlations between f_{Tr} and both precipitation and relative humidity suggest that higher precipitation and relative humidity promote transpiration fraction, whereas higher vapor pressure deficit reduces transpiration fraction. The positive correlation between f_{Ev} and temperature and vapor pressure deficit, and the negative correlation between f_{Ev} and relative humidity indicate that higher temperature and vapor pressure deficit promotes evaporation fraction, whereas higher relative humidity reduces the evaporation fraction. Our results show that contributions of recycled moisture (especially transpiration) to local precipitation play an important role in regional water resource redistribution in the arid and semi-arid region of northwestern China.

Key words: ecohydrology; Heihe River Basin; hydrogen and oxygen isotopes; isotopic mixing

model; recycled moisture; water resource redistribution

1. Introduction

Precipitation is a primary input for global and regional water cycles. In general, it comes from three moisture sources: antecedent atmospheric water vapor, lateral advection, and local evapotranspiration (Trenberth, 1999). Among these three moisture sources, terrestrial moisture produced by evapotranspiration (surface evaporation and plant transpiration), also known as recycled moisture, has been recognized as an important component of the atmospheric moisture balance (Savenije, 1995; Trenberth, 1999; Trenberth et al., 2003; Bisselink and Dolman, 2009; Seneviratne et al., 2010), and it plays an important role in the hydrological cycle (Trenberth, 1999; van der Ent et al., 2010, 2014; Zemp et al., 2014). In particular, moisture recycling plays an important role in hydrological processes across arid and semi-arid Asia (Hua et al., 2016; Wang et al., 2016a), where it provides local precipitation and supplements the scarce water resources (Davie, 2008; Jasechko et al., 2013; Kong et al., 2013; Hua et al., 2016).

The reported contributions of evapotranspiration to local precipitation in China varied widely across regions. Using a two-dimensional Eulerian method, van der Ent et al. (2010) revealed that evapotranspiration from eastern Eurasia contributed about 80% of the precipitation over China. The recycling ratio was 23% in the inland Shiyang River basin (where annual T_{mean} was 9°C) from May to October (Li et al., 2016). Recently, Wang et al. (2016a) calculated a recycling ratio of approximately 16.2% at large oases in the Urumqi region and less than 5% at small oases. Kong et al. (2013) reported that the recycling ratio was less than 2% in the Tianshan mountains (where annual T_{mean} was -3°C) and 15% in the Urumqi region over a year (where annual T_{mean} was 8°C). Surprisingly, the monthly maximum precipitation recycling ratio reached 62% on the southeastern

Qinghai-Tibet Plateau in July (Guo and Wang, 2014). Such a wide range of recycling ratios over different regions highlights the diverse factors that control precipitation recycling due to natural variations in hydro-meteorological conditions and in other factors such as topography (Trenberth, 1999; Peng et al., 2011; Kong et al., 2013) and the size of the spatial domain under consideration (Trenberth, 1999; Dominguez et al., 2006, 2008; Dominguez and Kumar, 2008). In addition, other factors, such as soil water content and land use and land cover change (Deng et al., 2015; Miralles et al., 2011), temperature and relative humidity (Peng et al., 2011), and the groundwater table and vegetation net primary productivity (Yao et al., 2018) might also affect the ratio of recycling precipitation by affecting soil evaporation and plant transpiration. The magnitudes of these effects and their interactions require further investigation. Researcher has investigated the origins of summer moisture in northwestern China from 1982 to 2010 (Hua et al., 2017). Previous studies have also investigated the sources of water vapor (e.g., Li et al., 2008; Huang et al., 2011; Zhao et al., 2011; Huang et al., 2015; Wang et al., 2015; Hua et al., 2017) and moisture transport processes (Simmonds et al., 1999; Li et al., 2008; Zhou & Huang, 2010; Huang et al., 2011; Chen & Huang, 2012) in arid and semi-arid regions of northwestern China. They found that the region's water vapor supply originated predominantly in Eurasia and was transported by the mid-latitude westerlies.

If precipitating vapor (the atmospheric vapor responsible for precipitation formation) can be assumed to represent an intensive mixture of advected and recycled vapor, the relative contributions of each flux (advection, surface evaporation, and transpiration) to the precipitation will be the same as those in the precipitating vapor, and the proportion of recycled moisture in precipitation can then be determined using multiple methods. These include analytical models (e.g., Dominguez et al., 2008; Pathak et al., 2014; Wei et al., 2016), numerical models (e.g., Bosilovich and Chern, 2006; Goessling

and Reick, 2011) and isotope-based models (e.g., Froehlich et al., 2008; Peng et al., 2011; Aemisegger et al., 2014; Li et al., 2016; Wang et al., 2016a).

In particular, the hydrogen (δ^2H) and oxygen ($\delta^{18}O$) stable isotope ratios can be used to analyze the water budget and calculate the contribution of recycled water to precipitation. If the isotopic compositions of moisture differ among fluxes of advection, soil evaporation, and plant transpiration, the relative contributions from these sources to precipitation can be determined using isotopic mixing models (Clark and Fritz, 1997; Genereux, 1998; Peng et al., 2011). Given that there are three dominant sources that contribute to precipitation, the three-component model (e.g., Phillips and Gregg, 2001; Peng et al., 2011) is suitable for distinguishing the relative contributions of advection, surface evaporation, and transpiration. Analysis in stable isotope compositions of local precipitation and advection source precipitation, plant xylem water (as a proxy of the transpiration moisture under the assumption of an isotopic steady-state on a scale of days, weeks, or longer time) and shallow soil water can be combined with models of the $\delta^{18}O$ and δ^2H values in evaporated water and advected moisture to estimate the proportion of recycled moisture in precipitation. Based on isotopic approaches, many studies have focused on contribution of evapotranspiration to local precipitation in China (Peng et al., 2011; Xu et al., 2011; Kong et al., 2013; Guo and Wang, 2014; Li et al., 2016; Wang et al., 2016a). Although these studies provided knowledge about the contribution of moisture recycling to local precipitation in northwestern China, they were conducted at relatively small spatial scales. In our literature review, we found few investigations that explored the contribution of recycled moisture to local precipitation over a large inland watershed. In the present study, one of our goals was to provide this information for a large and complex inland watershed, which included terrain ranging from upstream mountains with rich water resources to the extremely arid lower

reaches. In addition, more quantitative efforts are still necessary to examine the controlling factors of moisture recycling, especially in the inland river basin at the basin scale.

It is well established that evaporation changes the oxygen-18 (^{18}O) and deuterium (^{2}H) contents of the evaporated water (Craig and Gordon, 1965), thus, the deuterium excess (d-excess = $\delta^{2}H - 8 \times \delta^{18}O$; Dansgaard, 1964) of the evaporated vapor becomes higher than that of evaporating water (Salati et al., 1979; Gat and Matsui, 1991). The precipitation d-excess, with a worldwide average of 10‰, is an effective tracer for moisture sources (Clark and Fritz, 1997; Dansgaard, 1964; Gat and Carmi, 1970). It provides a measure of non-equilibrium isotopic effects and is primarily determined by kinetic fractionation during evaporation in the source region as a function of relative humidity, temperature, wind speed and other boundary layer properties (Clark and Fritz, 1997; Rozanski et al., 1993). The d-excess value can be modified by the mixing of inland water vapor derived from evapotranspiration (Gat et al., 1994; Liu et al., 2008) and by secondary evaporation (Fritz et al., 1987). Precipitation derived from marine moisture sources that evaporated under humid conditions has a relatively low d-excess, whereas that derived from recycled moisture evaporated under low humidity has a relatively high d-excess (Craig, 1961; Dansgaard, 1964; Merlivat and Jouzel, 1979; Machavaram and Krishnamurthy, 1995; Kurita and Yamada, 2008; Pang et al., 2011; Kaseke et al., 2018).

The Heihe River Basin is China's second-largest inland river basin. As a representative dryland inland river basin, the basin consists of three major topographic units. These units are the Qilian Mountains in the upper reaches, at the southern boundary of the basin; a corridor plain in the middle reaches, at the foot of the Qilian Mountains; and a broad northern plain in the lower reaches, bordering on low mountains and the Alashan Plateau in the Badain Jaran Desert and Mongolia.

Ecological degradation due to a combination of unsustainable human activities with climate change and a shortage of water have seriously threatened the sustainability of the basin's ecosystems (Wu et al., 2015; Yan et al., 2015). The basin's landscape includes the alpine steppe, alpine meadow, and forest ecosystems in the upper reaches; the artificial oasis, the desert-oasis ecotone and the Gobi (i.e., deserts with a gravel surface; We used the Gobi in our study) in the middle reaches; and the riparian forest, Gobi and desert in the lower reaches. The Heihe River Basin is a classic example of hydrological response to a combination of climate change and human activities. These different regions may play important but different roles in moisture recycling, and the contribution of moisture recycling cannot be ignored. However, we found no report on moisture recycling within the Heihe River Basin at a basin scale. Therefore, an integrated assessment of recycled moisture that includes both surface evaporation and transpiration is needed for this important basin. In the current study, we analyzed $\delta^{18}O$ and $\delta^{2}H$ of precipitation, soil water, and plant xylem water. Some of the data was supplemented by data from previous research: Zhao et al. (2018) for precipitation, Zhao et al. (2014) for soil and plant xylem water, and Yang et al. (2015) and Wen et al. (2016) for soil water and plant xylem water. We used these data to model the $\delta^{18}O$ and $\delta^{2}H$ of evaporation ($\delta^{18}O_{Ev}$ and $\delta^{2}H_{Ev}$), precipitating vapor ($\delta^{2}H_{PV}$ and $\delta^{18}O_{PV}$) and advected moisture ($\delta^{18}O_{Adv}$ and $\delta^{2}H_{Adv}$) using equilibrium fractionation theory, the modified Craig–Gordon equation and, an isotopic mixing model. Our goal was to better understand the dynamics of moisture recycling and the controlling factors within the second-largest inland river basin in northwestern China. We had four objectives: (1) to reveal seasonal and annual variations of $\delta^{2}H$ and $\delta^{18}O$ in the different water pools of the basin; (2) to employ the stable-isotope approach to quantitatively assess the extent of moisture recycling in the basin; (3) to estimate the relative contributions of moistures from advection and evapotranspiration to

precipitation in the basin's three topographic units; and (4) to examine the controlling factors of moisture recycling in the basin.

2. Materials and Methods

2.1. Study area

The Heihe River Basin has a drainage area of 130,000 km^2, and includes the upper reaches in the Qilian Mountains; the middle reaches, which include the Zhangye, Linze and Gaotai basins; and the lower reaches, which include the Jinta and Ejina basins (Figure 1a). The elevations of the upper, middle, and lower reaches ranged from 2000 to 5000 m, 1300 to 1700 m and 910 to 1450 m above sea level, respectively. The basin's climate is mainly controlled by the Westerlies throughout the year (Zhao et al., 2011; Yao et al., 2009).

Figure 1 Here

The mean annual temperature in the upper reaches of the Heihe River Basin ranges from -3.0 to 4.0°C, and the mean annual precipitation ranges from 200 mm to 600 mm. In the middle reaches, the mean annual temperature ranges from 3.0 to 7.0°C, and the mean annual precipitation ranges from 50 to 150 mm. In the lower reaches, the mean annual temperature is about 8°C, and the mean annual precipitation is only 42.0 mm. Figure 1b-f shows that precipitation mainly occurs in the summer months, from April to October, with very low winter precipitation. Table S1 summarizes the abbreviations and variable names used in our analysis.

2.2. Selection of the advection source for the precipitating vapor

Precipitation $\delta^{18}O$: The seasonal variations in precipitation $\delta^{18}O$ between the headwaters of the Heihe River Basin and the region affected by the Westerlies was similar (Yao et al., 2009; Zhao et al., 2011; Wang et al., 2016b), indicating that the moisture entering the headwaters of the basin was

derived predominantly from the Westerlies during summer and was derived predominantly from both the Westerlies and polar air masses during the winter (Figure 2; Yao et al., 2009; Zhao et al., 2011; Wang et al., 2016b). The long-term variability of monthly $\delta^{18}O$ values of precipitation at Urumqi (which is located in the northwest of the study area, at 87.62°E, 43.78°N, 918 m) from 1986 to 1992, 1995 to 1998, 2001 to 2003 (http://nds121.iaea.org/wiser), and 2012 to 2013 (Wang et al., 2016b) showed the same pattern and the mean values were similar during these periods (Yao et al., 2009; Wang et al., 2016b). In addition, similar $\delta^{18}O$ seasonal patterns and similar values were found at Urumqi and other cities on the northern slopes of the Tianshan Mountains, which are northwest of the study area (Yao et al., 2009; Wang et al., 2016b). Based on these data and the dominance of the Westerlies as a source of advected water vapor for the Heihe River Basin, we used the isotopic composition at Urumqi to represent the isotopic composition of the advection source in our calculations.

Figure 2 Here

NCEP/NCAR Reanalysis: To represent the regional wind fields, we used the reanalysis-derived wind field data for the Westerlies that were the dominant circulation that affected the seasonality of precipitation isotopes in the study region. We used the NCEP/NCAR reanalysis datasets (https://www.esrl.noaa.gov/psd/data/gridded/data.ncep.reanalysis.html) to calculate the wind fields and the geopotential height contours at 500 hPa in July 2009, 2011, 2012, and 2014 (Figure S1), which represent the summer moisture source areas for the Heihe River Basin. The geopotential height contours in the study region generally paralleled the latitude lines during the summer, and the wind speeds and directions were similar in July 2009, 2011, 2012, and 2014 in the basin (Figure S1). The winds originated primarily from the west. These results supported our choice of the Westerly air

masses as the water source for the Heihe River Basin and adjacent regions.

The Hybrid Single-Particle Lagrangian Integrated Trajectory (HYSPLIT) model: To identify the movement of bodies of air, we applied version 4 of the Hybrid Single-Particle Lagrangian Integrated Trajectory (HYSPLIT) model (Draxler and Hess, 1998; Draxler and Rolph, 2016). This approach has been widely applied to diagnose mass transport of air and to identify moisture sources (Soderberg et al., 2013; Bailey et al., 2015; Salamalikis et al., 2015; Zwart et al., 2016). Using this approach, we characterized mass transport of air and moisture sources for the Heihe River Basin (Figure S2). We found that the westerly fetch was dominant throughout the basin at all three heights that we modeled (500, 1000, and 1500 m above the ground surface).

Based on these meteorological analyses, the Urumqi site was a suitable source of data for the advection source that supplied precipitating vapor to the Heihe River Basin. At the Urumqi site, based on data from 1951 to 2009 (Figure 1), the annual precipitation totaled 267.0 mm, with monthly mean precipitation of 86.1 mm during the summer (June to August) and 33.1 mm during the winter (December to February). The mean annual temperature was 6.8°C, with monthly mean temperatures of 23.0°C during the summer and -11.7°C during the winter.

2.3. Stable isotope model for partitioning moisture sources of precipitation

According to the conceptual models of atmospheric moisture fluxes over land proposed by Brubaker et al. (1993) and van der Ent et al. (2010), a region's precipitation is sourced from both local evapotranspiration and moisture advected from elsewhere. The former includes moisture from surface evaporation and plant transpiration. In light of the isotopically distinct sources of moisture (Table S2), the stable isotopic compositions of the precipitation can be used to partition the moisture sources by using a dual-isotope (^{18}O and ^{2}H), three-end-member linear mixing model to determine

the contributions of each end-member (i.e., each moisture source). We assumed that the isotope composition of atmospheric water vapor, after accounting for precipitation in the region, is mixture of the isotopes in the moisture advected into the region by the prevailing air mass (here, the Westerlies) and the two types of moisture (evaporation and transpiration) that form evapotranspiration. The mass balance isotope-mixing model for $\delta^{18}O$ and $\delta^{2}H$ values can be expressed as follows (Genereux, 1998; Phillips and Gregg, 2001):

$$\delta^{18}O_{PV} = f_{Tr}\,\delta^{18}O_{Tr} + f_{Ev}\,\delta^{18}O_{Ev} + f_{Adv}\,\delta^{18}O_{Adv} \qquad (1a)$$

$$\delta^{2}H_{PV} = f_{Tr}\,\delta^{2}H_{Tr} + f_{Ev}\,\delta^{2}H_{Ev} + f_{Adv}\,\delta^{2}H_{Adv} \qquad (1b)$$

$$f_{Tr} + f_{Ev} + f_{Adv} = 1 \qquad (1c)$$

In equation (1), the fraction of each end-member is denoted as f, with subscripts PV for precipitating vapor, Tr for plant transpiration, Ev for surface evaporation, and Adv for advection. The corresponding $\delta^{18}O$ and $\delta^{2}H$ values represent the oxygen and hydrogen isotopic compositions. Our derivation of δ values for each component in equation (1) is described in the rest of this section.

In arid and semi-arid regions, the isotopic ratio of precipitation can be strongly affected by evaporation as the rain falls through the atmosphere. Thus, the precipitation is no longer in isotopic equilibrium with the vapor that it formed from. The process of sub-cloud evaporation will cause the observed precipitation to become progressively enriched in both ^{18}O and ^{2}H. To account for this effect, we corrected the isotopic ratio of precipitation (δ_P) in the Heihe River Basin and its advected vapor source (based on the values at Urumqi) using the method of Kong and Pang (2016):

$$\delta_{Pc} \cong \delta_P - (\alpha_{w-v} + \varepsilon_{kl-v})\ln(1 - f_e) \qquad (2)$$

where δ_{Pc} represents the corrected value in precipitation after a fraction (f_e) evaporated from the sub-cloud precipitation. The α_{w-v} is the enrichment factor from liquid water (precipitation) to vapor,

and ε_{kl-v} represents the kinetic enrichment factor from liquid water (precipitation) to vapor, respectively (Kong et al., 2013). The f_e is calculated as follows:

$$f_e = \frac{P}{P+V_{evap}t_{end}} \qquad (3)$$

where P is the precipitation amount. f_e is the fraction of the water-drop mass remaining after evaporation, which depends on the evaporation rate (V_{evap}), initial radius of the drop (see eq. 4), and the fall time of the drop (t_{end}). The evaporation rate of the falling drop was determined using the method of Kinzer and Gunn, (1951):

$$V_{evap} = 4\pi r(1+\frac{Ea}{s'})D(\rho_a - \rho_b) \qquad (4)$$

$$t_{end} = H / V \qquad (5)$$

where H is the rainfall height, V is the falling velocity, r is the radius of falling drops, Ea is a dimensionless quantity that measures the actual heat of vapor exchange, s′ represents the effective thickness of a shell around the drop, and ρ_a and ρ_b are the density at the surface of the falling drop and in the ambient air, respectively. The first term in eq. 4 $\left(4\pi r\left(1+\frac{Ea}{s'}\right)\right)$ is mainly determined by the drop size and the ambient temperature, and the second factor $(D(\rho_a - \rho_b))$ is determined by the humidity and temperature. Thus, the calculation of both factors requires information on the drop size, humidity and temperature (Kinzer and Gunn, 1951).

The falling time of the water drop can be calculated by the falling velocity and the distance between the cloud base and the ground, which determines the time available for acceleration. For the falling velocity, we used the relationship given by Best (1950):

$$V = 9.58\{1 - \exp[-(r / 0.885)^{1.147}]\} \qquad (6)$$

where r is the water drop radius, and we used a value of 0.402 mm in our study based on the value estimated during the summer by Zhang et al., (2009). The H value in upper reaches of the Heihe

River Basin was the difference between 4600 m (Wang et al., 2009) and altitude, and the H values at the other sites were calculated using $H = 5 - 0.075 \times (\varphi - 23)$, the relationship specified in ITU (International Telecommunications Union) (1992), where φ is the latitude (in decimal degrees). From V and H, we can estimate the fall time of the water-drop. Based on the meteorological data for the study sites (see section 2.4), the effect of sub-cloud evaporation can then be determined. In addition, during the process of sub-cloud evaporation, each droplet could have a different evaporation rate. But here, our 'droplet' is not the same as the actual droplet. It is more an equivalent droplet that could represent the average evaporation rate of the bulk rainfall. Previous research had assumed that the falling raindrops have a uniform spherical shape (Froehlich et al., 2008).

Because moisture transfer from land surface to the atmosphere by transpiration does not cause fractionation (Flanagan et al., 1991), δ_{Tr} is the same as the isotopic ratio in the local water used by plants, namely plant xylem water (δ_{Tr} equals the isotopic ratio of plant xylem water under the isotopic steady-state on a scale of days, weeks, or longer time). In this study, δ_{Tr} values of plant xylem water were sampled from the Heihe River Basin (Figure 1, Table 1).

The $\delta^{18}O_{PV}$ and $\delta^{2}H_{PV}$ values for precipitating vapor can be derived from the corrected isotopic values (δ_{Pc}) for the precipitation at the sampling location (Clark and Fritz, 1997; Kendall and Caldwell, 1998):

$$\delta_{PV} \cong \delta_{Pc} - 1000 \times (\alpha_{w-v} - 1) \qquad (7)$$

where α_{w-v} represents the equilibrium fractionation factors between water and vapor for oxygen and hydrogen isotopes. In equation (2), (7) and (8), α_{w-v} is a function of air temperature (T, in K) (the same as following equations from (10) to (12)), and δ_{PV} was corrected from δ_{Pc} by considering the fraction (f_e) of sub-cloud precipitation that evaporated. α_{w-v} was calculated as follows (Friedman and O'Neil, 1977; Criss, 1999):

$$10^3 \ln \alpha_{w-v} = 1.137(10^6/T^2) - 0.4156(10^3/T) - 2.0667 \quad \text{(8a: For } ^{18}\text{O)}$$

$$10^3 \ln \alpha_{w-v} = 24.844(10^6/T^2) - 76.248(10^3/T) + 52.612 \quad \text{(8b: For } ^{2}\text{H)}$$

In contrast, moisture that transfers from the land surface to the atmosphere by evaporation experiences strong fractionation, and the product vapor is depleted in heavy isotopes (Gat et al., 1994; Yepez et al., 2003). Craig and Gordon (1965) developed the following model to calculate the isotopic ratios of water vapor (δ_{Ev}) that evaporates from the soil surface:

$$\delta_{Ev} = \frac{\delta_{e/\alpha_{w-v}} - \delta_{PV} h - \varepsilon_{eq} - (1-h)\varepsilon_k}{(1-h) + (1-h)\varepsilon_k/1000} \quad (9)$$

where δ_e represents the $\delta^{18}O$ or $\delta^{2}H$ value in liquid water at the evaporating front, we estimated δ_{Ev} by measuring the isotope composition of shallow soil water (δ_e). δ_{PV} is the $\delta^{18}O$ or $\delta^{2}H$ value for the background atmospheric water vapor. The α_{w-v} for hydrogen or oxygen isotopes can be derived from equation (8), and is a function of shallow soil temperature (T, in K); $\varepsilon_{eq} = 1000(1 - [1 / \alpha_{w-v}])$; The ε_k is the kinetic fractionation associated with diffusion of water through the soil, and $\varepsilon_k = 1000(\alpha_k - 1)$, α_k (ε_k) with values of 1.0189 (~19‰) for oxygen and 1.017 (~17.0‰) for hydrogen in a turbulent boundary layer (Flanagan et al., 1991); and *h* is the relative humidity normalized based on the soil temperature at the evaporating front (Xu et al., 2008). We recorded soil temperature (°C) at depths of 5 and 10 cm in the upper reaches; 10 cm at the artificial oasis (Yang et al., 2015); 20 cm at the desert-oasis ecotone and Gobi in the middle reaches; and 10 cm in the lower reaches to correspond with the isotope data for the soil water.

In the Heihe River Basin, the precipitating vapor that accounts for the basin's precipitation was represented by the precipitation collected at each sampling station (PV-HRB, Figure 1). The isotope compositions of the precipitating vapor ($\delta_{PV\text{-}HRB}$) at each station can be derived from that of the precipitation at the sampling location ($\delta_{P\text{-}HRB}$) based on equations (7) and (8):

$$\delta_{PV-HRB} \cong \delta_{Pc-HRB} - 1000(\alpha_{w-v} - 1) \qquad (10)$$

The advected vapor (Adv) that contributes to the PV-HRB is the vapor sourced from the Westerly air masses at Urumqi (WU). We selected the Urumqi site as the source of the advected vapor (section 2.2). The isotope composition of precipitating vapor ($\delta_{PV\text{-}WU}$) that accounted for precipitation at the Urumqi site was calculated as follows:

$$\delta_{PV-WU} \cong \delta_{Pc-WU} - 1000(\alpha_{w-v} - 1) \qquad (11)$$

In equation (11), the monthly precipitation weighted average $\delta^{18}O_{P\text{-}WU}$ and $\delta^{2}H_{P\text{-}WU}$ values from 1986 to 1992, from 1995 to 1998 and from 2001 to 2003 (http://nds121.iaea.org/wiser) were used to calculate the $\delta^{18}O_{PV\text{-}WU}$ and $\delta^{2}H_{PV\text{-}WU}$, and the precipitating temperature was represented by the surface air temperature at the Urumqi meteorological station. Thus, the $\delta_{PV\text{-}WU}$ values of the PV-WU vapor were calculated according to $\delta^{2}H_{Pc\text{-}WU}$ and $\delta^{18}O_{Pc\text{-}WU}$ at Urumqi, respectively. As the PV-WU vapor flows into the Heihe River Basin from the west and becomes Adv vapor, the isotope composition of the moving PV-WU vapor experiences Rayleigh distillation-type isotope fractionation during condensation. Therefore, the isotope composition of the advected vapor that contributes to PV-WU can be estimated from the $\delta_{PV\text{-}WM}$ value by applying the Rayleigh distillation equation (Peng et al., 2011):

$$\delta_{\mathrm{Adv}} = \delta_{\mathrm{PV-WU}} - 1000(\alpha_{\mathrm{w-v}} - 1)\ln F \qquad (12)$$

where δ_{Adv} represents the isotope composition of the product vapor; $\delta_{PV\text{-}WU}$ represents the isotope composition of the reactant vapor. The $\alpha_{w\text{–}v}$ for hydrogen and oxygen isotopes is derived from equation (8). To determine δ_{Adv} at the rainfall height, we corrected T using the dry adiabatic lapse rate of 0.6°C per 100 m. F denotes the moisture ratio of product vapor to reactant vapor. In this study, F is defined by the ratio of the mean humidity mixing ratio in the HRB to that Urumqi according to their mean humidity mixing ratio under saturated condition at mean monthly temperature. For

example, in this study, the F value was estimated based on the temperature of the advected vapor source sites such as Urumqi and its corresponding mean humidity mixing ratio under saturated condition and the local temperature and its corresponding mean humidity mixing ratio under saturated condition of each sampling sites of the HRB. Based on the values of the relevant parameters, we calculated f_{Tr}, f_{Ev}, and f_{Adv} in terms of δ values in equation (1) using version 1.04 of the ISOERROR dual-isotope three-source mixing model (IsoSource software: http://www.epa.gov/wed/pages/models.htm) (Genereux, 1998; Phillips and Gregg, 2001; Peng et al., 2011). Based on the δ values of the precipitating vapor, transpired vapor, evaporated vapor, and advected vapor, we also calculated the standard deviations of these parameters, as well as the correlations (Pearson's *r*) between $\delta^{18}O$ and $\delta^{2}H$, the source proportions and their variances, the standard error (SEs), and the 95% confidence intervals of the source proportions.

The isotopic mixing model is based on the idea that the product results from well-mixed reactants (Hunt et al., 1998; Peng et al., 2011); that is, equation (1) is applicable if the precipitating vapor is a well-mixed moisture source consisting of transpiration, evaporation, and advection. Therefore, the subsequent rainfall that condenses from the precipitating vapor would inherit f_{Tr}, f_{Ev}, and f_{Adv} values obtained from precipitating vapor using ISOERROR (Genereux, 1998; Phillips and Gregg, 2001; Peng et al., 2011).

2.4. Sample collections and isotopic analysis

We complied a database of stable isotopic compositions of different water pools (precipitation, soil water, and plant water) throughout the Heihe River Basin based on our own observations (Zhao et al., 2014; Zhao et al., 2018), data from the Global Network of Isotopes in Precipitation (GNIP) of the International Atomic Energy Agency (http://nds121.iaea.org/wiser), and from the literature

(Huang and Wen, 2014; Wen et al., 2016). Table 2 provides details of the sampling sites shown in Figure 1.

2.4.1. Precipitation samples

Precipitation samples were collected at Yeniugou (P1), Hulugou (P2), and Pailugou (P3) in the upper reaches, at Zhangye (P4) in the middle reaches, and in the riparian forest at Ejina (P5) in the lower reaches (Figure 1, Table 1). The precipitation stable isotope compositions at Zhangye (P4) from 1986 to 2003 were obtained from the GNIP database (http://nds121.iaea.org/wiser). Data from May 2012 to September 2012 at Zhangye (P4) were obtained from Huang and Wen (2014). To prevent evaporation of the sampled water, rain samples for each precipitation event were collected and immediately transferred to fill air-tight 8 mL or 20-mL plastic bottles (Brand CNW, Germany). The solid samples (snow and hail) were collected and then melted in low-density polyethylene zip-lock bags at room temperature before being sealed into plastic bottles. We used new low-density polyethylene bags for each sample. All samples were stored at 6 to 8°C prior to analysis. The corresponding meteorological data were obtained from local weather stations (Figure 1), and included air and shallow soil temperature, relative humidity and, precipitation amount. In addition, we calculated the vapor-pressure deficit (*VPD*) using the mean air temperature (T_a, in degree Celsius) and mean relative humidity (*RH*):

$$VPD = \left(1 - \frac{RH}{100}\right) \times SVP \qquad (13)$$

where the saturated vapor pressure (*SVP*, kPa) is calculated as follows:

$$SVP = 0.6108 \times \exp\left(\frac{17.27 \times T_a}{T_a + 273.3}\right) \qquad (14)$$

2.4.2. Soil samples

We used 8.0 mL glass bottles to collect soil samples at 39 sites throughout the Heihe River

Basin (Figure 1, Table 2). In the upper reaches, we obtained 366 soil samples at depths of 0 to 5 cm and 5 to 10 cm soil at 22 sites (S1-S13 and W1-W9) from August 2007 to September 2011 (Figure 1 and Table 2). In the middle reaches, we sampled to depths of 10 or 20 cm, depending on the site. At the artificial oasis site (S14), data to a depth of 10 cm was cited and calculated using a regression equation for soil water $\delta^{18}O$ ($\delta^{2}H = 3.5\times\delta^{18}O - 26.6$) from Yang et al. (2015). For the desert-oasis ecotone sites (15-S19) and the Gobi sites (S20-S22), soil samples were taken to a depth of 10 cm (S15) or 20 cm (all other sites). In the lower reaches, soil samples were taken to a depth of 10 cm from riparian forest in the Ejina basin (S23-S30), and at the S24 site, 0-10cm soil samples were obtained at 2 h intervals from 06:00 on 6 August to 14:00 on August 9, 2009.

2.4.3. Plant samples

We obtained samples of plant xylem water from grasses, shrubs and, trees. Plant samples were taken from roots for grasses and from stems for shrubs and trees (Table 2). In the upper reaches, we obtained root samples of herbaceous plants such as *Stipa capillata* and *Polygonum viviparum* from mountain grassland, mountain meadow, grassland meadow and mountain grassland (S1–S4). The stem samples of Qinghai spruce (*Picea crassifolia*) and root samples of *Stipa capillata* and *Polygonum viviparum* were taken from forest sites (S5-S13). Sampling times for Qinghai spruce stems and *Stipa capillata* roots at S10, for Qinghai spruce and *Potentilla fruticosa* stems and *Polygonum viviparum* roots at S11 and S12, and for Qinghai spruce stems at P13 were the same as the soil sample collections at these sites (S10–S13). In the middle reaches,, root samples of maize (Yang et al., 2015) were taken from the artificial oasis (S14). Stem samples of *Tamarix ramosissima*, *Haloxylon ammodendron*, *Caragana Korshinskii*, *Populus gansuensis*, *Artemisia sphaerocephala* and *Calligonum mongolicum* were taken from the desert-oasis ecotone sites (S15-S19) and, stem of

Reaumuria songarica, *Nitraria schoberi* and *Calligonum mongolicum* were taken from the Gobi sites (S20-S22). At sites S16 and S20, stem samples of *Tamarix ramosissima* and *Haloxylon ammodendron*, and stem samples of *Reaumuria songarica* and *Nitraria schoberi* were taken from 06:00 on 15 June to 06:00 on 16 June 2010 and from 06:00 on 18 June to 06:00 on 19 June 2010, respectively. In the lower reaches,, stem samples of *Populus euphratica* and *Tamarix ramosissima* and root samples of *Sophora alopecuroides* were taken from sites S23 to S30 in riparian forest in the Ejina basin. At site S24, *Populus euphratica* stem samples and *Sophora alopecuroides* root samples were taken from 06:00 on 6 August to 12:00 on 9 August 2009. At sites S25 and S27, stems of *Populus euphratica*, roots of *Sophora alopecuroides*, and stems of *Tamarix ramosissima* were taken from 06:00 on 21 June to 06:00 on 22 June 2010. At S30, stems of *Populus euphratica* and *Tamarix ramosissima* and roots of *Sophora alopecuroides* were taken from 05:00 on 20 August to 21:00 on 21 August 2008. All plant tissues were collected at 2-hour intervals.

2.4.4. Water extraction and isotopic analysis

For the soil, root and, stem samples, we used samples from two 8 mL glass bottles (one for water extraction, and the other for a backup) to extract water. All samples were frozen at the field stations right after sampling and then transferred to the laboratory for water extraction. The samples were processed at the Key Laboratory of Ecohydrology of the Inland River Basin, Northwest Institute of Eco-Environment and Resources, Chinese Academy of Sciences. Water was extracted from roots, stem and, soils by means of cryogenic vacuum distillation (Ehleringer et al., 2000; West et al., 2006; Zhao et al., 2016), and extraction was performed under a 0.03-hPa vacuum for at least 2 h to ensure an unfractionated water sample (West et al. 2006). The resulting extracted water samples were sealed with Parafilm, placed in a bath and allowed to thaw. The liquid water was then

transferred into a 2 mL glass vial for $\delta^{18}O$ and $\delta^{2}H$ analysis. If the extracted water was less than 1 ml, we used glass-lined tubing embedded in the 2 ml glass vials.

The $\delta^{18}O$ and $\delta^{2}H$ values of the soil water and xylem water samples were measured using a Euro EA3000 element analyzer (HEKAtech, Wegberg, Germany) coupled to an Isoprime isotope ratio mass spectrometer (Isoprime Ltd., Cheadle Hulme, UK) at the Heihe Key Laboratory of Ecohydrology and River Basin Science, Northwest Institute of Eco-Environment and Resources, Chinese Academy Sciences. To avoid the memory effect associated with continuous-flow methods and assess the precision of the measurements, each sample was measured five times, and the first two values were discarded. The precision was better than ±1.0‰ for $\delta^{2}H$ and ±0.2‰ for $\delta^{18}O$. The $\delta^{18}O$ and $\delta^{2}H$ values of the precipitation samples were measured using an L2130-I analyzer (Picarro, Santa Clara, CA, USA), and the precision was better than ±0.5‰ for $\delta^{2}H$ and ±0.1‰ for $\delta^{18}O$. The $\delta^{18}O$ and $\delta^{2}H$ were calibrated using one international standard material and two lab working standards [BJD (lake water from the Badain Jaran Desert: $\delta^{2}H$ and $\delta^{18}O$ were -3.70‰ and 5.71‰, respectively), LZPW (ultrapure tap water from Lanzhou city, Gansu province, China: $\delta^{2}H$ and $\delta^{18}O$ were -67.7‰ and -8.2‰, respectively) and LZI (ultrapure groundwater from Lanzhou city: $\delta^{2}H$ and $\delta^{18}O$ were -82.1‰ and -11.2‰, respectively)] (Zhao et al. 2016). We first used three international standard materials: the Vienna Standard Mean Ocean Water (V-SMOW), Greenland Ice Sheet Precipitation (GISP) and, Standard Light Antarctic Precipitation (SLAP) as standards. We then selected three samples each to check their delta ranges of the soil water, precipitation, and xylem water samples, respectively. We selected one international standard and two of the three lab working standards for calibration purposes according to the sample delta ranges. For example, we used V-SMOW, BJD and, LZPW to calibrate the soil water data, used V-SMOW, LZPW and, LZI to calibrate the plant water

data, and used SLAP, BJD and, LZI to calibrate the precipitation, respectively. The $\delta^{18}O$ and $\delta^{2}H$ values are expressed in ‰ on the V-SMOW scale.

3. Results and Discussion

3.1. Variations of $\delta^{18}O$ and $\delta^{2}H$ in different water pools

3.1.1. Variations of $\delta^{18}O$ and $\delta^{2}H$ in precipitation

We observed significant seasonality of precipitation isotopes in our study area (Figure 2). Generally, the $\delta^{18}O$ and $\delta^{2}H$ values were higher in summer and lower in winter, which is in accordance with previous results for the region dominated by the Westerlies and our previous study using precipitation $\delta^{18}O$, the NECP/NCAR re-analysis data (National Centers for Environmental Prediction/National Center for Atmospheric Research) and, the HYSPLIT model (Tian et al., 2007; Kong and Pang, 2016; Zhao et al., 2011; Yao et al., 2009; Wang et al., 2016b). The similarity of the seasonality suggests that the mean precipitation $\delta^{18}O$ and $\delta^{2}H$ values reveal the similar origins of the moisture entering the Heihe River Basin (Figure S1). To more precisely determine the origin of the moisture entering the basin, we compared the seasonal variations in precipitation $\delta^{18}O$, $\delta^{2}H$ and d-excess for the basin with the values at Urumqi (which is also affected by the westerly air masses), and found similar seasonal variations, except d-excess in the Ejina Basin (Figure 2b) due to its extremely arid conditions and low precipitation (Figure 1f). This suggests the moisture sources are the same in our study area and at Urumqi and are mainly sourced from the Westerly circulation (Yao et al., 2009; Zhao et al., 2011). Therefore, it is acceptable to use Urumqi precipitation $\delta^{18}O$ and $\delta^{2}H$ data to model the isotopic compositions of the source moisture that is advected into our study area.

Except from May to July, precipitation $\delta^{18}O$ and $\delta^{2}H$ for the Heihe River Basin was generally more negative than that at Urumqi (Figure 2a, 2b), suggesting that ^{18}O and ^{2}H depletion of the

rainfall water occurred during long-distance transport (Siegenthaler and Oeschger, 1980). The d-excess of the in the upper reaches (17.8‰) was greater than the global average value of 10‰, which suggests that this water is not only related to the westerly moisture transport and cold temperatures during precipitation, but also to strong recycling of moisture (Craig, 1961; Dansgaard, 1964; Merlivat and Jouzel, 1979; Machavaram and Krishnamurthy, 1995; Kurita and Yamada, 2008; Pang et al., 2011). The lowest d-excess was found in the Ejina Basin (-3.2‰), where the precipitation is low and temperature is high (Figure 1f), suggesting that sub-cloud secondary evaporation is strong in the lower reaches.

Figure 3 Here

It has been well established that $\delta^{18}O$ and $\delta^{2}H$ in precipitation are linearly related (Craig, 1961; Dansgaard, 1964), and this relationship is known as the Global Meteoric Water Line (GMWL) or the Local Meteoric Water Lines (LMWL), depending on the scope of the study. These lines are useful in hydrometeorology for detecting the source/origin of the moisture. Using all the event-based data from the upper and lower reaches, and the monthly-weighted values in the middle reaches at Zhangye (http://nds121.iaea.org/wiser), we established the LMWLs for the Heihe River Basin (Figure 3). Except at Ejina basin with extremely arid conditions (Figure 1f), the slopes of the LMWLs from the upper reaches to the middle reaches decreased significantly (Figure 3), indicating that stronger secondary evaporation occurred due to decreasing precipitation and relative humidity and increasing temperature from the upper reaches to the middle reaches (Figure 1c-1e). In addition, previous studies revealed that the $\delta^{18}O$ values of precipitation exhibit a “temperature effect” in the northern Tibetan Plateau (Tian et al., 2003; Yu et al., 2008; Yao et al., 2013) and in parts of China dominated by the westerlies (Zhao et al., 2012; Wang et al., 2015). However, we found no significant

relationship between temperature and $\delta^{18}O$ during the raining season based on both event-precipitation data (Figure 4a-d) and weighted average monthly precipitation (Figure 4e-i). These results suggest that these abnormal relationships between temperature and $\delta^{18}O$ during the raining season are common within the Heihe River Basin. This result suggests that high amounts of recycled moisture affected the traditional positive relationships between $\delta^{18}O$ and temperature during the raining season.

Figure 4 Here

3.1.2 Variations of $\delta^{18}O$, $\delta^{2}H$ and $\delta^{18}O$-$\delta^{2}H$ in different water pools

Figure 5 shows the measured isotopic compositions of all the water samples in $\delta^{2}H$-$\delta^{18}O$ plots. In the upper reaches, $\delta^{2}H$ and $\delta^{18}O$ values in the xylem water averaged -48.3‰ and -5.9‰ in the alpine zone (Yeniugou and Hulugou), and -52.1‰ and -7.6‰ in the mid-mountain zone (Pailugou). In the middle reaches, $\delta^{2}H$ and $\delta^{18}O$ values in the xylem water averaged -45.2‰ and -6.0‰ in the artificial oasis, -50.9‰ and -4.5‰ in the desert-oasis ecotone, and -32.2‰ and 1.1‰ in the Gobi. In the lower reaches, $\delta^{2}H$ and $\delta^{18}O$ values in the xylem water averaged -52.5‰ and -5.8‰ in the riparian forest of the Ejina Basin. In the upper reaches, the mean $\delta^{2}H$ and $\delta^{18}O$ of shallow soil water were -31.5‰ and -5.4‰, respectively, in the alpine zone, and -44.3‰ and -6.3‰ in the mid-mountain zone. In the middle reaches, they were -48.4‰ and -6.2‰, respectively, in the artificial oasis,, -20.8‰ and 3.4‰, respectively, in the desert-oasis ecotone, and -15.4‰ and 5.2‰, respectively, in the Gobi. In the lower reaches, they were -32.0‰ and 0.3‰, respectively, in riparian forest in the Ejina Basin. These results indicate that evaporation of soil water increased from the upper reaches to the lower reaches due to increasing temperature and decreasing precipitation (Figure 1c-1f).

The δ^2H and $\delta^{18}O$ of the plant xylem water and shallow soil water were negative in the upper reaches, and their δ^2H -$\delta^{18}O$ plots were on or close to the LMWL (Figure 5), suggesting that soil water and the water source of the corresponding dominant plants were recharged by local precipitation, and that weak evaporation occurred due to the low temperature and high relative humidity (Figure 1c, d). In the middle reaches, the δ^2H and $\delta^{18}O$ of plant xylem water and surface soil water from the artificial oasis were negative, and their δ^2H-$\delta^{18}O$ plots were on or close to the LMWL due to agricultural irrigation (552.9 mm during the 2012 growing season; Wen et al., 2016). In the Gobi, the δ^2H and $\delta^{18}O$ values for the plant xylem and shallow soil water were positive. Compared to the plant xylem water, the soil water δ^2H and $\delta^{18}O$ values were farther from the LMWL, indicating a strong evaporation effect, and this suggested that the dominant plants took up the deep soil water or groundwater (Zhou et al., 2017). In the lower reaches, the δ^2H and $\delta^{18}O$ of plant xylem water were more negative than those of the soil water, indicating that strong evaporation occurred and that the water source for the dominant plants was deep water and groundwater provided by river recharge and irrigation (Zhao et al., 2008; Ruan et al., 2014). These differences in plant xylem water and shallow soil water in the Heihe River Basin revealed differences in soil evaporation effects and plant water uptake due to the different climatic conditions, and these variations altered the δ^2H and $\delta^{18}O$ values of moisture produced by the soil evaporation and by plant transpiration. This, in turn, would have substantial effects on the local moisture recycling characteristics. In addition, we found negative δ^2H and $\delta^{18}O$ values of plant xylem water in the artificial oasis and desert-oasis ecotone in the middle reaches, and in the riparian forest in the river's lower reaches. These results suggest that human activities such as irrigation with groundwater or surface water with negative δ^2H and $\delta^{18}O$ values occurred in the middle reaches and that river water recharge supplied water to the riparian

forest in the lower reaches, thereby affecting the plant isotope compositions.

Figure 5 Here

3.2. Fraction of recycled moisture in the Heihe River Basin

3.2.1. Spatial variations

In the upper reaches, the highest contribution of recycled moisture to local precipitation occurred from June to August at Yeniugou, from May to August at Hulugou, and from June to September at Pailugou (Table 3). The recycled moisture in local precipitation (f_{Tr} + f_{Ev}) for these months combined averaged 55.3% at Yeniugou, 58.3% at Hulugou and 44.5% at Pailugou, which are similar to the value of 50% (ranging 43% to 54%) reported by Cheng et al. (2002) based on a water budget approach. The transpiration fractions (f_{Tr}) averaged 51.7% at Yeniugou, 52.4% at Hulugou and 43.6% at Pailugou, and the evaporation fractions (f_{Ev}) averaged 3.6% at Yeniugou, 5.9% at Hulugou and 0.9% at Pailugou (Table 3, Table S2, Figure 6). These results suggest that advected vapor and transpiration moisture contribute approximately the same amount of water to local precipitation during these corresponding periods in the upper reaches. This agrees with a previous study at a high elevation, which showed that transpiration accounted for most of the recycled moisture and that evaporation represented only a minor contribution (Peng et al., 2011).

Figure 6 Here

In the middle reaches, the average contribution of recycled moisture to local precipitation was 45.7% in the artificial oasis, 56.4% in the desert-oasis ecotone, and 21.4% in the Gobi, versus f_{Tr} values of 36.1, 12.2, and 15.1%, respectively, and f_{Ev} values of 9.5, 44.3, and 6.3%, respectively (Table 3, Table S2, Figure 6). The artificial oasis, desert-oasis ecotone, and Gobi are close to each other (Figure 1), but their transpiration fractions differed greatly. This suggests that human activities

such as reclamation of the artificial oasis (Lu et al., 2015), changing the land cover or land use (Deng et al., 2015), increasing the relative humidity and water supply through irrigation (Shi et al., 2011; Yao et al., 2018), and changing plant traits such as leaf area index by changing the vegetation type (Huang and Wen, 2014; Zhou et al., 2018) can all affect the recycling characteristics through their effects on soil evaporation and plant transpiration. It is interesting that there were similar proportions of recycled moisture to local precipitation in the artificial oasis and desert-oasis ecotone, but these values resulted from different mechanisms. At the artificial oasis, f_{Tr} played the dominant role in local precipitation due to strong transpiration under high vegetation coverage during growing season (Maize, Huang and Wen (2014)). However, f_{Ev} at the desert-oasis ecotone was nearly equal to f_{Adv}, probably due to irrigation combined with low vegetation cover in this region. To validate our estimates, we compared our results with the results of Kong et al. (2013) in the arid Urumqi catchment in Xinjiang province since the physical environment in the desert-oasis ecotone is mostly similar to that at Urumqi. Our estimated f_{Ev} is almost four times of f_{Tr} at the desert-oasis ecotone, which also agrees with a comparable study in the arid Urumqi catchment in Xinjiang (Kong et al., 2013), where vast coverage of desert region exists, and the evapotranspiration should be mainly composed of evaporation.

In the lower reaches, f_{Tr} was 25.6% in the riparian forest of the Ejina Basin, whereas f_{Ev} was negative according to our model. This may be related to the extremely low soil moisture that developed under extremely arid conditions (Figure 1f). The advection fraction was 83.7% at the riparian forest (Table 3, Table S2, Figure 6). Our results suggest that the three-end-member linear mixing model must be improved to better account for the conditions in extremely arid regions.

During September and October at Yeniugou and Hulugou, and during May and September at

Pailugou, the contributions of recycled moisture to precipitation were 16.3, 32.7, and 19.4%, whereas the contributions of advected vapor were 83.7, 67.3 and 80.6%, respectively, indicating that advected vapor was the major source of precipitation during May, September and October. In addition, compared to Gobi in the middle reaches, we found higher transpiration in the artificial oasis of the middle reaches and in the riparian forest of the lower reaches, and higher evaporation fractions in the desert-oasis ecotone of the middle reaches. These results indicate that human activity changed local moisture recycling by changing land cover or land use (Deng et al., 2015), vegetation coverage and plant species (Huang and Wen, 2014), the amount of soil moisture through irrigation (Shi et al., 2011) and water delivery (Cheng et al., 2014; Hu et al., 2015; Zhang et al., 2018).

3.2.2. Seasonal variations

We found different seasonal patterns for the fractions of precipitation contributed by transpiration (f_{Tr}) and evaporation (f_{Ev}) fractions to local precipitation in the Heihe River Basin (Table 3, Figure 7a, b). In the alpine zone of the upper reaches (at Hulugou and Yeniugou), the seasonal patterns of f_{Tr} were similar, and high f_{Tr} occurred from May to July. However, the forest zone at Pailugou showed a different pattern, with low values in May, increasing to high values from June to September, following the temperature trends, suggesting that temperature was the main factor that controlled transpiration in the upper reaches. For f_{Ev}, there was no obvious seasonality in the upper reaches, with values < 10% throughout the study period.

In the middle reaches, f_{Tr} showed similar seasonality in the artificial oasis, desert-oasis ecotone, and Gobi, with the highest f_{Tr} in July and the highest value in the artificial oasis, suggesting that the variations in land cover and land use (Deng et al., 2015), and in vegetation coverage and plant species (Huang and Wen, 2014), controlled transpiration in the artificial oasis. f_{Ev} was highest in the

desert-oasis ecotone throughout the study period (Table 3, Figure 7b). This is likely related to the fact that there is more irrigated water to evaporate and lower plant cover in this ecosystem. In the artificial oasis and Gobi, f_{Ev} values were similar and showed a similar pattern, with values decreasing gradually from May to September, but for different reasons. In the artificial oasis, the, high vegetation density would reduce soil evaporation during the growing season (e.g., Wang et al. 2013), whereas in the Gobi, the extremely arid conditions produce a water supply that is insufficient to support continuous evaporation. However, f_{Ev} for the Gobi reached its lowest values in August and September, possibly because of increasing depletion of soil water during the growing season. In the riparian forest of the lower reaches, f_{Tr} was much higher in May and September than from June to August (Table 3, Figure 7a). This may be because water diversion from the middle reaches to the lower reaches occurs in May and September to sustain the *Populus euphratica* forest and maintain the water level in Juyan lake, in the Ejina Basin.

Overall, the seasonal variations of f_{Tr} and f_{Ev} in the Heihe River Basin were complex and were affected by multiple anthropogenic factors that interacted with variations of physical factors such as temperature, precipitation, and relative humidity (Figure 1c-f).

Figure 7 Here

3.3. Factors that control the recycling fraction

Many factors control evapotranspiration, including the soil water content, topography, land use or land cover, irrigation, light supply, temperature, relative humidity, wind velocity, plant species, vegetation coverage and leaf area index. Soil evaporation and plant transpiration have been extensively estimated as a function of soil moisture and land cover (Mu et al., 2007; Pelgrum et al., 2010; Brolsma et al., 2010). Many such studies have used satellite observation-based soil moisture

datasets to estimate soil evaporation and transpiration (Mu et al., 2009; Miralles et al., 2011; Bastiaanssen et al., 2012). Zhou et al. (2018) confirmed that transpiration to evapotranspiration ratio (T/ET) varied consistently with leaf area index for individual ecosystems in the Heihe River Basin, which is consistent with the global pattern (Wang et al., 2014). Due to data constraints, we only analyzed how four meteorological factors (temperature, precipitation, relative humidity, and vapor pressure deficit) control the contributions of transpiration and evaporation to precipitation (Figure 8). We found no significant relationship between temperature and f_{Tr} at the basin scale (Figure 8a; $p = 0.121$, $n = 60$). However, we found a significant positive relationship using all data from the upper reaches, with a slope of $2.15\%\cdot{}^{\circ}C^{-1}$, suggesting that temperature promotes the transpiration fraction under the natural, well-watered, and cold conditions in the upper reaches. However, we found no significant relationship in the middle and lower reaches, likely do to simultaneous interactions among multiple factors. For example, in the artificial oasis in the middle reaches, high f_{Tr} (especially from June to September) was related to the growth of crops and the use of irrigated agriculture (Deng et al., 2015; Zhang et al., 2018), whereas the low f_{Tr} of the desert-oasis ecotone was related to the low vegetation coverage, and the low f_{Tr} of the Gobi was related to the extremely low vegetation coverage and dry soil. Moreover, we found significant relationships between relative humidity and f_{Tr} at the basin scale when we only included values of relative humidity >40% (i.e., excluding May 2012 in the artificial oasis and desert-oasis ecotone in the middle reaches and in the riparian forest in the lower reaches) (Figure 8b; $R^2 = 0.417$, $p < 0.001$) and between precipitation and f_{Tr} (Figure 8c) ($R^2 = 0.205$, $p < 0.001$). These results suggest that higher precipitation and relative humidity promote plant transpiration in arid and semi-arid regions (Peng et al., 2011) by improving water conditions. We also found a significant negative relationship between vapor pressure deficit and f_{Tr} at the basin

scale (Figure 8d; R^2 = 0.140, p = 0.004), indicating that a high vapor pressure deficit limits transpiration in arid and semi-arid regions. Among the climate factors, temperature had the strongest effect on f_{Tr}, with a slope of 2.150%·°C^{-1} in the upper reaches (Figure 8a), followed by relative humidity (0.992%·°C^{-1}) for relative humidity >40% (Figure 8b).

Figure 8 Here

Figure 9 Here

When we excluded data from the desert-oasis ecotone, we found several statistically significant relationships. We found a positive relationship between f_{Ev} and temperature (R^2 = 0.327, p < 0.001, n = 41, with a slope of 0.377%·°C^{-1}; Figure 9a). We found a statistically significant negative correlation between f_{Ev} and relative humidity (R^2 = 0.146, p = 0.014, n = 41, with a slope of 0.117%·%$^{-1}$; Figure 9b). We also found a significant positive relationship between f_{Ev} and vapor pressure deficit (R^2 = 0.440, p < 0.001, *n* = 41, with a slope of 6.640%·kPa^{-1}; Figure 9c). These results revealed that higher temperature and vapor pressure deficit increases f_{Ev} by increasing soil evaporation, whereas higher humidity reduces f_{Ev}. Unfortunately, we lack leaf area index and soil moisture data for our study sites, so we can't analyze their effects on f_{Tr} and f_{Ev}. In future research, it will be important to obtain such data to provide a more direct explanation for our results.

3.4. Evaluation of the isotope-based recycling fractions

The mass balance isotope-mixing model can directly estimate the moisture-recycling fraction in local precipitation, thereby avoiding the need to estimate the highly uncertain amount of evapotranspiration that is needed in a typical water budget analysis. The isotope approach can also divide the recycling fraction into its respective transpiration and evaporation components. However, any method has its own uncertainty. In this study, we evaluated the uncertainty of the isotope-based

method from three perspectives: the uncertainties in measurements and modeled results, the sensitivities analysis for the parameters (here, using the Monte Carlo method), and the 95% confidence intervals of our estimates (using the method of Phillips and Gregg, 2001). Table 3 and 4 summarizes the results.

First, we evaluated the effects of instrument precision. The precision was better than ± 1.0‰ for δ^2H and ± 0.2‰ for $\delta^{18}O$ in our analysis of the soil and xylem water, and better than ± 0.5‰ for δ^2H and ± 0.1‰ for $\delta^{18}O$ in the precipitation samples. Based on our results, transpiration accounted for more of the recycled moisture than evaporation at all sample sites except the desert-oasis ecotone. With values <10% at most sites, evaporation plays a minor role, and transpiration plays an important role in local precipitation. We used the $\delta^{18}O_{Tr}$ and δ^2H_{Tr} values at Pailugou, in the upper reaches, to evaluate the effects of instrument precision because of the availability of long-term precipitation data and intensive soil and plant sampling at this site (Tables 1 and 2). With the other parameters kept constant, we calculated f_{Tr}, f_{Ev} and f_{Adv} based on the mean $\delta^{18}O_{Tr}$ ± 0.2 and the mean δ^2H_{Tr} ± 1 (Table S3). Compared to the f_{Tr}, f_{Ev} and f_{Adv} results modeled with the mean $\delta^{18}O_{Tr}$ and δ^2H_{Tr}, the differences in f_{Tr}, f_{Ev} and f_{Adv} when modeled with mean $\delta^{18}O_{Tr}$ - 0.2 and δ^2H_{Tr} - 1.0 were -0.4, 0.2, and 0.2% respectively, versus 0.4, -0.2, and -0.2% when modeled with $\delta^{18}O_{Tr}$ + 0.2 and δ^2H_{Tr} + 1.0, respectively (Table S3). Thus, the impact of these changes is minimal. Because we used isotopic data from soil water and xylem water (for the dominant plants) collected near the precipitation sites, we are confident these data can represent changes in the local precipitation, soil water, and plant conditions. We also selected the Pailugou results to evaluate our modeled results by altering the isotopic ratio of the transpiration flux by ± 1‰ for $\delta^{18}O_{Tr}$ and by ± 8‰for δ^2H_{Tr} (assuming a constant d-excess). With the other parameters kept constant, we then calculated the f_{Tr}, f_{Ev} and f_{Adv} values

based on mean $\delta^{18}O_{Tr} \pm 1$ and $\delta^{2}H_{Tr} \pm 8$ (Table S4). Compared to the f_{Tr}, f_{Ev} and f_{Adv} results modeled with the mean $\delta^{18}O_{Tr}$ and $\delta^{2}H_{Tr}$, the differences in f_{Tr}, f_{Ev} and f_{Adv} when modeled with $\delta^{18}O_{Tr}$ - 1 and $\delta^{2}H_{Tr}$ - 8 were -3.0, -0.1, and 2.9%, respectively, and were 2.6, -0.1, and -2.5% when modeled with $\delta^{18}O_{Tr}$ + 1 and $\delta^{2}H_{Tr}$ + 8, respectively (Table S4). Based on Figure 5, the ranges of $\delta^{18}O_{Tr}$ and $\delta^{2}H_{Tr}$ at Pailugou were large, so these differences will be proportionally small, and the ranges of $\delta^{18}O_{Tr}$ and $\delta^{2}H_{Tr}$ at other sites should be affected even less. This means that the stable isotope approach can be used to assess the extent of moisture recycling in the Heihe River Basin during the growing season with reasonable reliability.

Other factors could potentially cause uncertainties in the estimates of isotopic compositions of different components such as the variations in the condensation temperature and the kinetic effects associated with soil evaporation. We did not quantify the sensitivities of our results to these factors due to a lack of data, but we used the Monte Carlo method to indirectly evaluate the effects of such uncertainties on the recycling estimates. In our study, we used the standard deviations of $\delta^{18}O_{Tr}$ and $\delta^{2}H_{Tr}$, $\delta^{18}O_{Ev}$ and $\delta^{2}H_{Ev}$, $\delta^{18}O_{PV}$ and $\delta^{2}H_{PV}$, and $\delta^{18}O_{Adv}$ and $\delta^{2}H_{Adv}$ to evaluate the uncertainty using the Monte Carlo method with 10,000 iterations (Table 4). The values of f_{Tr} and f_{Ev} were close to those from our model, especially during the growing season. During the active growing seasons, the bias estimated by Monte Carlo method ranged from 4.1% to 5.9% for f_{Tr} at Yeniugou, Hulugou, and Pailugou, versus 6.1% at the artificial oasis, suggesting that during the active growing season and under conditions of high vegetation coverage and abundant water, our performed well for modeling $f_{Tr.}$ The bias was higher at the other sites and other growing season, possibly due to the different sampling periods and the extremely arid conditions. For f_{Ev}, the uncertainties of the model are relatively large. We also found relatively large uncertainties for the desert-oasis ecotone, Gobi, and

the riparian forest, especially in the riparian forest, where f_{Tr} was negative. This provides a reminder of the need to be cautious when the model is used in extremely arid regions, where more work needs to be done to improve the model's performance.

Based on these uncertainty evaluations, there is still room to improve the isotopic modeling. For examples, some limitations were described by Peng et al. (2011), including a lack of measurements of the isotope compositions of water vapors, as well as the isotopic compositions of moisture from evaporation and transpiration. Some of these limitations can be solved by improved measuring techniques. For example, the $\delta^{18}O_{PV}/\delta^{2}H_{PV}$ (Risi et al., 2010; Huang and Wen, 2014), $\delta^{18}O_{Tr}/\delta^{2}H_{Tr}$ (Wang et al., 2012) and $\delta^{18}O_{Ev}/\delta^{2}H_{Ev}$ of soil (Soderberg et al., 2012) can be measured either directly by isotope ratio infrared spectroscopy, or by coupling isotope ratio infrared spectroscopy with various chambers (Wang et al., 2012). However, how to attain more accurate $\delta^{18}O_{Adv}/\delta^{2}H_{Adv}$ and $\delta^{18}O_{Ev}/\delta^{2}H_{Ev}$ values for shallow groundwater and surface water in basins with different river systems and flow areas will require further research to find improvements. In addition, we only measured or modeled the $\delta^{18}O$ and $\delta^{2}H$ of water vapor in the lowest part of the atmosphere. By assuming that these measurements are representative of water vapor throughout the vertical atmosphere, we likely risk overestimating the contribution of evapotranspiration. However, we believe this risk is small because water vapor content in the upper layers is very low in the semi-arid to arid environments of our study area in northwest China.

4. Conclusions

Our uncertainty analysis suggests that the three-end-member linear mixing model we employed can quantitatively assess the extent of moisture recycling in the Heihe River Basin. Our results suggest that transpiration accounts for more of the recycled moisture than evaporation, which has a

relatively low contribution to precipitation at all sites except the desert-oasis ecotone. During the active growing season, the mean recycled moisture percentage in the Qilian Mountains (52.4%) was similar to that in the desert-oasis ecotone (56.5%), and higher than those in the artificial oasis (21.4%) and Gobi (21.4%) in the middle reaches of the Heihe River and in the Ejina Basin in the lower reaches (25.6%). In addition, the transpiration fraction of recycled moisture was higher in the Qilian Mountains (49.0%) than in the artificial oasis (36.1%), the desert-oasis ecotone (12.2%), and the Gobi (15.1%) in the middle reaches and higher than in the riparian forest in the lower reaches (25.6%). This indicates that meteorological factors, vegetation coverage, plant species, and human activities such as changes in land cover and land use, irrigation, and water delivery are major factors that affect the contribution of evapotranspiration to local precipitation.

In some regions, the transpiration fraction of recycled moisture differed significantly. For example, human activities alter the contribution of recycled moisture to local precipitation in the artificial oasis and desert-oasis ecotone by changing the land cover and land use, and the water and heat conditions through irrigation and water delivery. In addition, except in the middle and lower reaches of the Heihe River Basin, which are affected by human activities, higher temperature appears to promote transpiration in the upper reaches, and increase the evaporation fractions at a basin scale, whereas higher precipitation and relative humidity to enhance transpiration and reduce evaporation fractions on the basin scale. In addition, higher vapor pressure deficit decreased transpiration fractions and increased evaporation fractions (except in the desert-oasis ecotone) at a basin scale.

The isotope-based approach is an effective method to model the moisture recycling in the upper reaches and in the artificial oasis in the middle reaches, but the modeling results were not ideal in the desert-oasis ecotone and Gobi in the middle reaches, and in the riparian forest in the lower reaches,

where the climate is dry and plant coverage is relatively low. Moreover, the isotope-based approach has limitations related to uncertainties in the isotopic compositions of the different water pools. However, as the measurement techniques improve, the model's estimates will improve, thereby providing more accurate estimates of the contributions of recycled moisture to precipitation in arid and semi-arid inland river basin.

Acknowledgments

This study was supported by the National Natural Science Foundation of China (Grant No. 41571025, 41730751 and 41771028), the Shaanxi province natural science foundation research project (2016JM4006), and the Key Laboratory of Agricultural Water Resources, the Chinese Academy of Sciences (No. KFKT201606). Lixin Wang acknowledges support from the Division of Earth Sciences of National Science Foundation (NSF EAR-1554894) and the President's International Research Awards from Indiana University. We thank staff of the Qilian Alpine Ecology and Hydrology Research Station and the Linze Inland River Basin Research Station, Northwest Institute of Eco-Environment and Resources, Chinese Academy of Sciences, for assistance with the precipitation sampling and the meteorological data. All data are available in the supporting information (Table S2).

References

Aemisegger, F., Pfahl, S., Sodemann, H., Lehner, I., Seneviratne, S.I., Wernli, H., 2014. Deuterium excess as a proxy for continental moisture recycling and plant transpiration. Atmos. Chem. Phys. 14, 4029–4054.

Bailey, H.L., Kaufman, D.S., Henderson, A.C.G., Leng, M.J., 2015. Synoptic scale controls on the $\delta^{18}O$ in precipitation across Beringia. Geophys. Res. Lett., 42, 4608–4616.

Bastiaanssen, W.G.M., Cheema, M.J.M., Immerzeel, W.W., Miltenburg, I.J., Pelgrum, H., 2012. Surface energy balance and actual evapotranspiration of the transboundary Indus Basin estimated from satellite measurements

and the ETLook model. Water Resour. Res. 48, W11512. https://doi.org/10.1029/2011WR010482.

Best, A.C., 1950. Empirical formulae for the terminal velocity of water drops falling through the atmosphere. Quart. J. Roy. Meteor. Soc. 76, 302-311.

Bisselink, B., Dolman, A.J., 2009. Recycling of moisture in Europe: contribution of evaporation to variability in very wet and dry years. Hydrol. Earth Syst. Sci. 13, 1685–1697.

Bosilovich, M.G., Chern, J.D., 2006. Simulation of water sources and precipitation recycling for the MacKenzie, Mississippi, and Amazon River Basins. J. Hydrometeorol. 7, 312–329.

Brolsma, R.J., Karssenberg, D., Bierkens, M.F.P., 2010. Vegetation competition model for water and light limitation. I: model description, one-dimensional competition and the influence of groundwater. Ecol. Modell. 221 (10), 1348–1363.

Brubaker, K.L., Entekhabi, D., Eagleson, P.S., 1993. Estimation of continental precipitation recycling. J. Clim. 6, 1077–1089.

Chen, G.S., Huang, R.H., 2012. Excitation mechanisms of the teleconnection patterns affecting the July precipitation in Northwest China. J. Clim. 25, 7834–7851. https://doi.org/10.1175/JCL1-D-11-00684.1.

Cheng, G.D., Li, X., Zhao, W.Z., Xu, Z.M., Feng, Q., Xiao, S.C., Xiao, H.L., 2014. Integrated study of the water–ecosystem–economy in the Heihe River Basin. Nat. Sci. Rev. 1, 413–428.

Cheng, J.D., Lin, L.L., Lu, H.S., 2002. Influences of forests on water flows from headwater watersheds in Taiwan. For. Ecol. Manage. 165, 11–28. https://doi.org/10.1016/S0378-1127(01)00626-0.

Clark, I.D., Fritz, P., 1997. Environmental Isotopes in Hydrogeology. CRC Press, Boca Raton, Florida.

Craig, H., 1961. Isotopic variation in meteric waters. Science 133 (3465), 1702– 1703.

Craig, H., Gordon L.I., 1965. Deuterium and oxygen-18 variations in the ocean and the marine atmosphere. In E. Tongiorgi (ed.), Proceedings of the Conference on Stable Isotopes in Oceanographic Studies and Paleotemperatures. Laboratory of Geology and Nuclear Science, Pisa, pp. 9-121.

Criss, R.E., 1999. Principles of Stable Isotope Distribution. Oxford Univ Press, New York.

Dansgaard, W., 1964. Stable isotopes in precipitation. Tellus, 16, 436-468.

Davie, T., 2008. Fundamentals of Hydrology. Routledge Press, New York.

Deng, X.Z., Shi, Q.L., Zhang, Q., Shi, C.C., Yin, F., 2015. Impacts of land use and land cover changes on surface energy and water balance in the Heihe River Basin of China, 2000–2010. Phys. Chem. Earth Parts A/B/C, 79–82, 2-10.

Dominguez, F., Kumar, P., 2008. Precipitation recycling variability and ecoclimatological stability—A study using

NARR data. Part I: Central U. S. plains ecoregion. J. Clim. 21(20), 5165–5186. https://doi.org/10.1175/2008JCLI1756.1.

Dominguez, F., Kumar, P., Liang, X., Ting, M., 2006. Impact of atmospheric moisture storage on precipitation recycling. J. Clim. 19(8), 1513–1530. https://doi.org/10.1175/JCLI3691.1.

Dominguez, F., Kumar, P., Vivoni, E.R., 2008. Precipitation recycling variability and ecoclimatological stability—A study using NARR data. Part II: North American Monsoon region. J. Clim. 21(20), 5187–5203. https://doi.org/10.1175/2008JCLI1760.1.

Draxler, R.R., Hess, G.D., 1998. An overview of HYSPLIT_4 modelling system for trajectories, dispersion and deposition. Aust. Meteorol. Mag. 47, 295–308.

Draxler, R.R., Rolph, G.D., 2016. HYSPLIT (HYbrid Single-Particle Lagrangian Integrated Trajectory) Model, NOAA Air Resources Laboratory. [Available at http://www.arl.noaa.gov/HYSPLIT.php.]

Ehleringer, J.R., Roden, J., Dawson, T.E., 2000. Assessing ecosystem-level water relations through stable isotope ratio analyses. In Methods in Ecosystem Science, pp. 181–198. Springer, Verlag New York.

Flanagan, L.B., Comstock, J.P., Ehleringer, J.R., 1991. Composition of modeled and observed environmental influences on the stable oxygen and hydrogen isotope composition of leaf water in Phaseolus vulgaris L. Plant Physiol. 96, 588–596.

Friedman, I., O'Neil, J.R., 1977. Compilation of stable isotope fractionation factors of geochemical interest. J. Chem. Inf. Model. 53, 160.

Fritz, P., Morgan, A.V., Eicher, U., McAndrews, J.H., 1987. Stable isotope, fossil coleoptera and pollen stratigraphy in late quaternary sediments from Ontario and New York state. Palaeogeogr. Palaeoclimatol. Palaeoecol. 58(3–4): 183-202. https://doi.org/10.1016/0031-0182(87)90059-9.

Froehlich, K., Kralik, M., Papesch, W., Rank, D., Scheifinger, H., Stichler, W., 2008. Deuterium excess in precipitation of Alpine regions-moisture recycling. Isotopes Environ. Health S. 44, 61–70.

Gat, J.R., Bowser., C.J., Kendall, C., 1994. The contribution of evaporation from the Great Lakes to the continental atmosphere: Estimate based on stable isotope data. Geophys. Res. Lett., 21, 557–560.

Gat, J.R., Carmi, I., 1970. Evolution of the isotopic composition of atmospheric waters in the Mediterranean Sea area. J. Geophys. Res. 75 (15), 3039–3048.

Gat, J.R., Matsui, E., 1991. Atmospheric water balance in the Amazon basin: an isotopic evapo-transpiration model. J. Geophys Res. 96(D7), 13179-13188.

Genereux, D., 1998. Quantifying uncertainty in tracer-based hydrograph separations. Water Resour. Res. 34,

915–919.

Goessling, H.F., Reick, C.H., 2011. What do moisture recycling estimates tell us? Exploring the extreme case of non-evaporating continents, Hydrol. Earth Syst. Sci. 15, 3217–3235. https://doi.org/10.5194/hess-15-3217-2011.

Guo, Y.P., Wang, C.H., 2014. Trends in precipitation recycling over the Qinghai–Xizang Plateau in last decades. J. Hydrol. 517, 826-835.

Hu, X.L., Lu, L., Li, X., Wang, J.H., Guo, M., 2015. Land use/cover change in the middle reaches of the Heihe River Basin over 2000–2011 and its implications for sustainable water resource management. PLoS One, 10, e0128960.

Hua, L.J., Zhong, L.H., Ke, Z.J., 2016. Precipitation recycling and soil–precipitation interaction across the arid and semi-arid regions of China. Internat. J. Climatol. 36(11), 3708–3722. https://doi.org/10.1002/joc.4586.

Hua, L.J., Zhong, L.H., Ma, Z.G., 2017. Decadal transition of moisture sources and transport in northwestern China during summer from 1982 to 2010. J. Geophys. Res. Atmos. 122, 12, 522–12. https://doi.org/ 10.1002/2017JD027728.

Huang, G., Yong, L., Huang, R.H., 2011. The interannual variability of summer rainfall in the arid and semiarid regions of Northern China and its association with the Northern Hemisphere circumglobal teleconnection. Adv. Atmos. Sci. 28, 257–268. https://doi.org/10.1007/s00376-010-9225-x.

Huang, L.J., Wen, X. F., 2014. Temporal variations of atmospheric water vapor δD and $\delta^{18}O$ above an arid artificial oasis cropland in the Heihe River Basin. J. Geophys. Res–Atmos. 119, 11456-11476.

Huang, W., Feng, S., Chen, J.H., Chen, F.H., 2015. Physical mechanisms of summer precipitation variations in the Tarim Basin in Northwestern China. J. Clim. 28(9), 3579–3591. https://doi.org/10.1175/JCLI-D-14-00395.1.

Hunt, R.J., Bullen, T.D., Krabbenhoft, D.P., Kendall, C., 1998. Using stable isotopes of water and strontium to investigate the hydrology of a natural and a constructed wetland. Ground Water, 36, 434–443.

ITU (International Telecommunications Union) ITU-R Recommendation PN. 839, Rain height model for prediction methods, 1992

Jasechko, S., Sharp, Z.D., Gibson, J.J., Birks, S.J., Yi, Y., and Fawcett, P.J., 2013. Terrestrial water fluxes dominated by transpiration. Nature, 496, 347–351.

Kaseke, K.F., Wang, L., Wanke, H., Tian, C., Lanning, M., Jiao, W., 2018. Precipitation origins and key drivers of precipitation isotope (^{18}O, ^{2}H, and ^{17}O) compositions over Windhoek. J. Geophys. Res–Atmos. 123.

Kendall, C., Caldwell, E.A., 1998. Fundamentals of isotope geochemistry, in Isotope Tracers in Catchment

Hydrology, edited by C. Kendall and J. J. McDonnell, pp. 51–86, Elsevier Press, Amsterdam.

Kinzer, G.D., Gunn, R., 1951. The evaporation, temperature and thermal relaxation-time of freely falling water drops. J. Meteorol. 8, 71-83.

Kong, Y.L., Pang Z.H., 2016. A positive altitude gradient of isotopes in the precipitation over the Tianshan Mountains: Effects of moisture recycling and sub-cloud evaporation. J. Hydrol. 542, 222-230.

Kong, Y.L., Pang, Z.H., Froehlich, K., 2013. Quantifying recycled moisture fraction in precipitation of an arid region using deuterium excess. Tellus 65B, 388-402.

Kurita, N., Yamada, H., 2008. The role of local moisture recycling evaluated using stable isotope data from over the middle of the Tibetan Plateau during the monsoon season. J. Hydrometeorol. 9 (4), 760–775.

Li, W.L., Wang, K.L., Fu, S.M., Jiang, H., 2008. The interrelationship between regional westerly index and the water vapor budget in Northwest China [in Chinese]. J. Glaciol. Geocryol. 30(1), 28–34.

Li, Z.X., Feng, Q. Wang, J., Kong, Y.L., Cheng, A.F., Yong, S., Li, Y.G., Li, J.G., Guo, X.Y., 2016. Contributions of local terrestrial evaporation and transpiration to precipitation using $\delta^{18}O$ and D-excess as a proxy in Shiyang inland river basin in China. Global Planet Change, 146, 140-151.

Liu, Z.F., Tian, L.D., Chai, X.R., Yao, T.D., 2008. A model-based determination of spatial variation of precipitation $\delta^{18}O$ over China. Chem. Geol. 249: 203-212.

Lu, Z.X., Wei, Y.P., Xiao, H.L., Zou, S.B., Xie, J., Ren, J., Western, A., 2015. Evolution of the human–water relationships in the Heihe River basin in the past 2000 years. Hydrol. Earth Syst. Sci. 19, 2261–2273.

Machavaram, M.V., Krishnamurthy, R.V., 1995. Earth surface evaporative process: A case study from the Great Lakes region of the United States based on deuterium excess in precipitation. Geochim Cosmochim Acta, 59, 4279–4283.

Merlivat, L., Jouzel, J., 1979. Global climatic interpretation of the deuterium-oxygen 18 relationship for precipitation. J. Geophys. Res. 84 (C8), 5029–5033.

Miralles, D., Holmes, T., de Jeu, R.A.M., Gash, J., Meesters, A., Dolman, A., 2011. Global land-surface evaporation estimated from satellite-based observations. Hydrol. Earth Syst. Sci. 15, 453–469.

Mu, Q., Heinsch, F.A., Zhao, M., Running, S.W., 2007. Development of a global evapotranspiration algorithm based on MODIS and global meteorology data. Remote Sens. Environ. 111, 519–536.

Mu, Q.Z., Jones, L.A., Kimball, J.S., McDonald, K.C., Running, S.W., 2009. Satellite assessment of land surface evapotranspiration for the Pan-Arctic domain. Water Resour. Res. 45, W09420. https://doi.org/10.1029/2008WR007189.

Pang, Z.H., Kong, Y.L., Froehlich, K., Huang, T.M., Yuan, L.J., Li, Z.Q., Wang, F.T., 2011. Processes affecting isotopes in precipitation of an arid region. Tellus B 63 (3), 352–359.

Pathak, A., Ghosh, S., Kumar, P., 2014. Precipitation recycling in the Indian Subcontinent during summer monsoon. J. Hydrometeorol. 15, 2050–2066.

Pelgrum, H., Miltenburg, I., Cheema, M., Klaasse, A., Bastiaanssen, W., 2010. ETLook a novel continental evapotranspiration algorithm. In: Remote Sensing and Hydrology Symposium, Jackson Hole, Wyoming, USA, 1085, 1087.

Peng, H., Mayer, B., Norman, A., Krouse, H.R., 2005. Modeling of hydrogen and oxygen isotope compositions for local precipitation, Tellus B, 57, 273–282. https://doi.org/10.1111/j.1600-0889.2005.00145.x.

Peng, T.R., Liu, K.K., Wang, C.H., Chuang, K.H., 2011. A water isotope approach to assessing moisture recycling in the island-based precipitation of Taiwan: A case study in the western Pacific. Water Resour. Res. 47, W08507. https://doi.org/10.1029/2010WR009890.

Phillips, D.L., Gregg, J.W., 2001. Uncertainty in source partitioning using stable isotopes. Oecologia 127, 171–179.

Risi, C., Bony, S., Vimeux, F., Frankenberg, C., Noone, D., 2010. Understanding the Sahelian water budget through the isotopic composition of water vapor and precipitation. J. Geophys. Res. 115, D24110.

Rozanski, K., Araguás-Araguás, L., Gonfiantini, R., 1993. Isotopic pattern in modern global precipitation. In: Swart, P.K., Lohwan, K.L., Mckenzie, J., Savin, S. (Eds.), Climate Change in Continental Isotopic Record. American Geophysical Union, Washington DC, pp. 1–36.

Ruan, Y.F., Zhao, L.J., Xiao, H.L., Cheng, G.D., Zhou, M.X., Wang, F., 2014. Water sources of plants and groundwater in typical ecosystems in the lower reaches of the Heihe River Basin. Sci. Cold Arid Reg. 6(3), 0226–0235.

Salamalikis, V., Argiriou, A.A., Dotsika, E., 2015. Stable isotopic composition of atmospheric water vapor in Patras, Greece: A concentration weighted trajectory approach. Atmos. Res. 152: 93–104.

Salati, E., Dall'Olio, A., Matsui, E., Gat, J.R., 1979. Recycling of water in the Amazon basin: an isotopic study. Water Resour. Res. 15, 1250–1258.

Savenije, H.H.G., 1995. New definitions or moisture recycling and the relationship with land-use changes in the Sahel, J. Hydrol. 167, 57–78.

Seneviratne, S.I., Corti, T., Davin, E.L., Hirschi, M., Jaeger, E.B., Lehner, I., Orlowsky, B., Teuling, A.J., 2010. Investigating soil moisture climate interactions in a changing climate: a review. Earth-Sci. Rev. 99, 125–161.

Shi, M. J., Wang, L., Wang, X.J., 2011. A study on changes and driving factors of agricultural water supply and

demand in Zhangye after water reallocation of the Heihe River. Resour. Sci. 33, 1489–1497 [in Chinese].

Siegenthaler, U., Oeschger, H., 1980. Correlation of ^{18}O in precipitation with temperature and altitudes. Nature 285: 314–318.

Simmonds, I., Bi, D., Hope, P., 1999. Atmospheric water vapor flux and its association with rainfall over China in summer. J. Clim. 12(5), 1353–1367. https://doi.org/10.1175/1520-0442(1999)012%3C1353:AWVFAI%3E2.0.CO;2.

Soderberg, K., Good, S.P., O'Connor, M., Wang, L.X., Ryan, K., Caylor, K.K., 2013. Using atmospheric trajectories to model the isotopic composition of rainfall in central Kenya. Ecosphere 4 (3), 331-341.

Soderberg, K., Good, S.P., Wang, L.X., Caylor, K., 2012. Stable isotopes of water vapor in the vadose zone: A review of measurement and modeling techniques. Vadose Zone J. 11(3). https://doi.org/10.2136/vzj2011.0165.

Tian, L.D., Yao, T.D., MacClune, K., White, J.W.C., Schilla, A., Vaughn, B., Vachon, R., Ichiyanagi, K., 2007. Stable isotopic variations in west China: a consideration of moisture sources. J. Geophys. Res. 112, 3–5.

Tian, L.D., Yao, T.D., Schuster, P.F., White, J.W.C., Ichiyanagi, K., Pendall, E., Pu, J.C., Yu, W.S., 2003. Oxygen-18 concentrations in recent precipitation and ice cores on the Tibetan Plateau. J. Geophys. Res. 108(D9), 4293. https://doi.org/10.1029/2002JD002173.

Trenberth, K.E., 1999. Atmospheric moisture recycling: role of advection and local Evaporation. J. Clim. 12, 1368–1381.

Trenberth, K.E., Dai, A., Rasmussen, R.M., Parsons, D.B., 2003. The changing character of precipitation. Bull. Am. Meteorol. Soc. 84, 1207–1217.

van der Ent, R.J., Savenije, H.H.G., Schaefli, B., Steele-Dunne S.C., 2010. Origin and fate of atmospheric moisture over continents. Water. Resour. Res. 46, W09525.

van der Ent, R.J., Wang-Erlandsson, L., Keys, P.W., Savenije, H.H.G., 2014. Contrasting roles of interception and transpiration in the hydrological cycle – Part 2: Moisture recycling. Earth Syst. Dyn. 5, 471–489.

Wang, L., Niu, S., Good, S., Soderberg, K., Zhou, X., Xia, J., Sherry, R., Luo, Y., Caylor, K. ,McCabe, M., 2013. The effect of warming on grassland evapotranspiration partitioning using laser-based isotope monitoring techniques. Geochimica et Cosmochimica Acta 111, 28-38.

Wang, L., Good, S.P., Caylor, K.K., 2014. Global synthesis of vegetation control on evapotranspiration partitioning. Geophys. Res. Lett. 41, 6753–6757.

Wang, L.X., Good, S.P., Caylor, K.K., Cernusak, L.A., 2012. Direct quantification of leaf transpiration isotopic

composition. Agric. For. Meteorol. 154/155, 127-135.

Wang, N.L., He, J.Q., Jinag, X., Song, G.J., Pu, J.C., Wu, X.B., Chen, L., 2009. Study on the zone of maximum precipitation in the north slopes of the central Qilian Mountains. J Glaciol. Geocryol. 31(3), 395-403

Wang, S.J., Zhang, M.J., Che, Y.J., Chen, F.L., Qiang, F., 2016a. Contribution of recycled moisture to precipitation in oases of arid central Asia: a stable isotope approach. Water. Resour. Res. 52, 3246–3257.

Wang, S.J., Zhang, M.J., Chen, F.L., Che, Y.J., Du, M.X., Liu, Y.M., 2015. Comparison of GCM simulated isotopic compositions of precipitation in arid central Asia. J. Geogr. Sci. 25 (7), 771–783.

Wang, S.J., Zhang, M.J., Hughes, C.E., Zhu, X.F., Dong, L., Ren, Z.G., Chen, F.L., 2016b. Factors controlling stable isotope composition of precipitation in arid conditions: An observation network in the Tianshan Mountains, central Asia. Tellus B 68, 289-299. http://doi.org/10.3402/tellusb.v68.26206.

Wei, J.H., Knoche, H.R., Kunstmann, H., 2015. Contribution of transpiration and evaporation to precipitation: An ET-Tagging study for the Poyang Lake region in Southeast China, J. Geophys. Res. Atmos., 120(14), 6845–6864. https://doi.org/10.1002/2014JD022975.

Wei, J.H., Knoche, H.R., Kunstmann, H., 2016. Atmospheric residence times from transpiration and evaporation to precipitation: An age-weighted regional evaporation tagging approach. J. Geophys. Res. Atmos., 121, 6841–6862. https://doi.org/10.1002/2015JD024650.

Wen, X.F., Yang, B., Sun, X.M., Lee, X., 2016. Evapotranspiration partitioning through in-situ oxygen isotope measurements in an oasis cropland. Agric. For. Meteorol. 230-231, 89-96.

West, A.G., Patrickson, S.J., Ehleringer, J.R., 2006. Water extraction times for plant and soil materials used in stable isotope analysis. Rapid Commun. Mass Spectrom. 20, 1317–1321.

Wu, F., Zhan, J.Y., Chen, J.C., He, C., Zhang, Q., 2015. Water yield variation due to forestry change in the head-water area of Heihe river basin, Northwest China. Adv. Meteorol. 1-8.

Xu, Y., Kang, S., Zhang, Y., Zhang, Y., 2011. A method for estimating the contribution of evaporative vapor from Nam Co to local atmospheric vapor based on stable isotopes of water bodies, Chin. Sci. Bull. 56, 1511–1517. https://doi.org/10.1007/s11434-011-4467-2.

Xu, Z., Yang, H., Liu, F., An, S., Cui, J., Wang, Z., Liu, S., 2008. Partitioning evapotranspiration flux components in a subalpine shrubland based on stable isotopic measurements. Bot. Stud. 49(4): 351-361.

Yan, H.M., Zhan, J.Y., Jiang, Q.O., Yuan, Y.W., Li, Z.H. 2015. Multilevel modeling of NPP change and impacts of water resources in the Lower Heihe River Basin. Phys. Chem. Earth 79-82, 29-39.

Yang, B., Wen, X.F., Sun, X.M., 2015. Seasonal variations in depth of water uptake for a subtropicalconiferous

plantation subjected to drought in an East Asian monsoon region. Agric. For. Meteorol. 201, 218-228.

Yao T.D., Zhou, H., Yang, X.X., 2009. Indian monsoon influences altitude effect of $\delta^{18}O$ in precipitation/river water on the Tibetan Plateau. Chin. Sci. Bull. 54, 2724-2731.

Yao, T.D., Masson-Delmotte, V., Gao, J., Yu, W.S., Yang, X.X., Risi, C., Sturm, C., Werner, M., Zhao, H.B., He, Y., Ren, W., Tian, L.D., Shi, C.M., Hou, S.G., 2013. A review of climatic controls on $\delta^{18}O$ in precipitation over the Tibetan Plateau: Observations and simulations. Rev. Geophys. 51(4), 525-548. https://doi: 10.1002/rog.20023.

Yao, Y.Y., Tian, Y., Andrews, C., Li, X., Zheng, Y., Zheng, C.M., 2018. Role of groundwater in the dryland ecohydrological system: A case study of the Heihe River Basin. J. Geophys. Res.: Atmos. 123, 6760-6776. https://doi.org/10.1029/2018JD028432.

Yepez, E.A., Williams, D.G., Scott, R.L., Lin, G.H., 2003. Partitioning overstory and understory evapotranspiration in a semiarid savanna woodland from the isotopic composition of water vapor. Agric. For. Meteorol. 119, 53–68.

Yu, W., Yao, T., Tian, L., Ma, Y., Ichiyanagi, K., Wang, Y., Sun, W., 2008. Relationships between $\delta^{18}O$ in precipitation and air temperature and moisture origin on a south-north transect of the Tibetan Plateau. Atmos. Res. 87(2), 158-169.

Zemp, D. C., Schleussner, C.F., Barbosa, H.M.J., van der Ent, R.J., Donges, J.F., Heinke, J., Sampaio, G., Rammig, A. 2014. On the importance of cascading moisture recycling in South America. Atmos. Chem. Phys., 14, 13,337–13,359. https://doi.org/10.5194/acp-14-13337-2014.

Zhang, G.Q., Sun, A.P., Zhou, W.F., Wang, L.J., Xiao, H.B., 2009. Preliminary Study on the Character of Raindrop Spectrum and Precipitation Mechanism in Menyuan of Qinghai. Plateau Meteorol. 28(1), 77-84.

Zhang, M.M., Wang, S., Fu, B.J., Gao, G.Y., Shen, Q., 2018. Ecological effects and potential risks of the water diversion project in the Heihe River Basin. Sci. Total. Environ. 619–620, 794-803.

Zhao, L.J., Eastoe, C.J., Liu, X.H., Wang, L.X., Wang, N.L., Xie, C., Song, Y.X., 2018. Origin and residence time of groundwater based on stable and radioactive isotopes in the Heihe River Basin, northwestern China. J. Hydrol-Regional Studies 18, 31-49.

Zhao, L.J., Wang, L.X., Cernusak, L.A., Liu, X.H., Xiao, H.L., Zhou, M.X., Zhang, S.Q., 2016. Significant Difference in Hydrogen Isotope Composition Between Xylem and Tissue Water in *Populus Euphratica*. Plant Cell Environ. 39, 1848–1857.

Zhao, L.J., Wang, L.X., Xiao, H.L., Ruan, Y.F., Zhou, M.X., Wang, F., 2014. The patterns and implications of

diurnal variations in d-excess of plant water, shallow soil water and air moisture. Hydrol. Earth Syst. Sci. 18, 4129-4151.

Zhao, L.J., Xiao, H.L., Cheng, G.D., Song, Y.X., Zhao, L., Li, C.Z., Yang, Q., 2008. A preliminary study of water sources of riparian plants in the lower reaches of the Heihe Basin. Acta Geoscientia Sinica 29(6), 709–718.

Zhao, L.J., Xiao, H.L., Zhou, M.X., Wang, L.X., Cheng, G.D., Ren, J., 2012. Factors controlling spatial and seasonal distributions of precipitation $\delta^{18}O$ in China. Hydrol. Process. 25(25): 1906-2015.

Zhao, L.J., Yin, L., Xiao, H.L., Cheng, G.D., Zhou, M.X., Yang, Y.G., Li, C.Z., Zhou, J., 2011. Isotopic evidence for the moisture origin and composition of surface runoff in the headwaters of the Heihe River basin. Chin. Sci. Bull. 56, 406–416.

Zhou, H., Zhao, W.Z., Zhang, G.F., 2017. Varying water utilization of *Haloxylon ammodendron* plantations in a desert-oasis ecotone. Hydrol. Process. 31(4), 825–835.

Zhou, L.T., Huang, R.H., 2010. Interdecadal variability of summer rainfall in Northwest China and its possible causes. Internat. J. Climatol. 30, 549–557. https://doi.org/10.1002/joc.1923.

Zhou, S., Yu, B.F., Zhang, Y., Huang, Y.F., Wang, G.Q., 2018. Water use efficiency and evapotranspiration partitioning for three typical ecosystems in the Heihe River Basin, northwestern China. Agric. For. Meteorol. 253–254, 261–273.

Zwart, C., Munksgaard, N.C., Kurita, N., Bird, M.I., 2016. Stable isotopic signature of Australian monsoon controlled by regional convection. Quaternary Sci. Rev. 151, 228-235.

Tables

Table 1

Location and characteristics of the precipitation sampling sites in the study area. Figure 1 shows their locations.

Region	Sampling sites	Site ID	Longitude (°E)	Latitude (°N)	Elevation (m asl)	Study dates	Data type
Upper reaches	Yeniugou	P1	99.63	38.70	3320	June 2008 to **Sept.** 2009	Event precipitation data
	Hulugou	P2	99.87	38.25	3020	July 2009 to Sept. 2009 May 2014 to Oct. 2014	Event precipitation data
	Pailugou	P3	100.28	38.57	2720	June 2011 to Oct. 2014	Event precipitation data
Middle reaches	Zhangye **and Linze**	P4	100.43	38.93	1483	1986 to 2003 (**http://nds121.iaea.org/wiser**)	Monthly weighted average rainfall
			100.37	38.85	1550	May 2012 to Sept. 2012 (Huang and Wen, 2014)	Event precipitation data
Lower reaches	Ejina	P5	101.10	41.97	920	Jan. 2007 to Dec. 2010	Event precipitation data

Table 2

Locations and details of the sampling sites shown in Figure 1. Plant species in the upper reaches: SC, *Stipa capillata*; PV, *Polygonum viviparum*; QS, Qinghai spruce (Picea crassifolia); and PF, *Potentilla fruticosa*. Plant species in the middle reaches: CK, *Caragana korshinskii*; PG, *Populus gansuensis*; TR, *Tamarix ramosissima*; HA, *Haloxylon ammodendron*; AS, *Artemisia sphaerocephala*; and CM, *Calligonum mongolicum* at the desert-oasis ecotone; and RS, *Reaumuria songarica*; NS, *Nitraria schoberi*, *and* CM, *Calligonum mongolicum* at the Gobi. Plant species in the lower reaches: PE, *Populus euphratica*; and SA, *Sophora alopecuroides*.

Region	Site ID	**Ecosystem type**	**Longitude (°E)**	**Latitude (°N)**	**Elevation (m asl)**	**Soil sample depth**	**Plant samples (species and tissue)**	**Study dates**
Upper reaches	W1	Mountain grassland	99.9	38.2	3349	0-10 cm	/	Aug. – Sept. 2009; May – July 2010
	W2		99.9	38.3	3098	0-10 cm	/	
	W3		99.9	38.3	3023	0-10 cm	/	
	W4		99.9	38.3	3023	0-10 cm	/	
	W5		99.9	38.3	3059	0-10 cm	/	
	W6		99.9	38.3	3005	0-10 cm	/	
	W7		99.9	38.2	/	0-10 cm	/	
	W8		99.9	38.2	/	0-10 cm	/	
	W9		99.9	38.2	/	0-10 cm	/	
	S1	Mountain grassland	99.9	38.8	2774	0-10 cm	SC - root	7 June 2009
	S2	Mountain grassland	99.9	38.8	3040	0-10 cm	PV - root	8 June 2009
	S3	Grassland meadow	99.6	38.6	3732	0-10 cm	SC - root	8 June 2009
	S4	Mountain grassland	99.9	38.8	3040	0-10 cm	PV - root	21 Aug. 2007
	S5	Mid-mountain forest	100.3	38.6	2594	0-10 cm	QS - stem	7 June 2009
	S6		99.6	38.8	2654	0-10 cm	QS - stem	8 June 2009
	S7		100.3	38.5	2774	0-10 cm	QS - stem	3 Aug. 2009
	S8		99.8	38.8	3006	0-10 cm	QS - stem	7 June 2009
	S9		100.3	38.6	2780	0-10 cm	QS - stem	1 Aug. 2012

	S10					Mean of 0-5 cm and 5-10 cm	QS - stem; SC - root	06:00 on 27 June 2011 to 18:00 on 28 June 2011
	S11		100.3	38.5	2900	Mean of 0-5 cm and 5-10 cm	QS and PF - stem; PV - root	06:00 on 23 June 2011 to 18:00 on 25 June 2011
	S12					Mean of 0-5 cm and 5-10 cm		08:00 on 6 Sept. 2011 to 17:00 on 8 Sept. 2011
	S13		100.3	38.0	2774	Mean of 0-5 cm and 5-10 cm	QS - stem	08:00 on 1 Aug. 2009 to 18:00 on 3 Aug. 2009
Middle reaches	S14	Artificial oasis	100.4	38.9	1550	Mean of 0-5 cm and 5-10 cm	Maize - root	Yang et al. (2015); Wen et al. (2016)
	S15	Desert-oasis ecotone	100.1	39.3	1380	0-10 cm	CK, TR, and PG - stem	31 July 2007
	S16		100.1	39.4	1386	0-20 cm	TR and HA - stem	06:00 on 15 June 2010 to 06:00 on 16 June 2010
	S17					0-20 cm	TR and HA - stem	3 Aug. 2012
	S18		100.1	39.4	1406	0-20 cm	HA - stem	4 Aug. 2012
	S19		100.1	39.4	1419	0-20 cm	HA, AS, and CM - stem	4 Aug. 2007
	S20	Gobi	100.1	39.4	1413	0-20 cm	RS and NS - stem	06:00 on 18 June 2010 to 06:00 on 19 June 2010
	S21					0-20 cm	RS and NS - stem	5 Aug. 2007
	S22		100.1	39.4	1384	0-20 cm	CM and NS - stem	3 Aug. 2007
Lower reaches	S23	Riparian forest	101.2	42.0	930	0-10 cm		19 June 2007
	S24					0-10 cm	PE - stem; SA - root	06:00 on 6 Aug. 2009 to 12:00 on 9 Aug. 2009
	S25					0-10 cm		06:00 on 21 June 2010 to 06:00 on 22 June 2010
	S26					0-10 cm	PE - stem	8 Aug. 2012
	S27					0-10 cm	TR - stem	06:00 on 21 June 2010 to 06:00 on 22 June 2010
	S28					0-10 cm		8 Aug. 2012
	S29		101.1	42.0	920	0-10 cm	PE and TR - stem; SA - root	05:00 on 20 Aug. 2008 to 21:00 on 21 Aug. 2008
	S30					0-10 cm		

Table 3

Seasonal variations of the moisture fractions from transpiration (f_{Tr}), evaporation (f_{Ev}), and advection (f_{Adv}) and their 95% confidence intervals at Yeniugou, Hulugou, and Pailugou in the upper reaches of the Heihe River Basin; in the artificial oasis, desert-oasis ecotone, and Gobi in the middle reaches; and in riparian forest in the Ejina Basin in the lower reaches. S.D. indicates the standard deviation.

Region	Site	Elevation (m asl)	Month		f_{Ev} (%) (S.D.)	f_{Tr} (%) (S.D.)	f_{Adv} (%) (S.D.)
Upper reaches	Yeniugou	3320	**June**	Source proportion (%)	**3.7 (6.2)**	**63.1 (3.2)**	**33.1 (6.9)**
				95% Confidence interval(%)	0-16.4	56.6-69.7	18.8-47.5
			July	Source proportion (%)	**2.3 (4.6)**	**55.6 (2.9)**	**42.1 (4.4)**
				95% Confidence interval (%)	0-11.6	49.9-61.3	33.1-51.0
			August	Source proportion (%)	**4.6 (6.4)**	**37.0 (6.0)**	**58.3 (4.0)**
				95% Confidence interval (%)	0-17.7	24.3-49.7	49.9-66.7
			September	Source proportion (%)	**5.3 (3.4)**	**9.4 (6.5)**	**85.3 (3.5)**
				95% Confidence interval (%)	0-12.1	0-22.5	78.1-92.4
			October	Source proportion (%)	**7.6 (0.8)**	**10.0 (1.1)**	**82.4 (0.4)**
				95% Confidence interval (%)	5.6-9.6	6.8-13.1	81.3-83.5
	Hulugou	3020	**May**	Source proportion (%)	**7.5 (8.7)**	**56.8 (4.2)**	**35.7 (8.7)**
				95% Confidence interval (%)	0-25.0	45.0-64.0	19.0-60.0
			June	Source proportion (%)	**6.5 (6.8)**	**54.9 (3.6)**	**38.6 (7.2)**
				95% Confidence interval (%)	0-21.0	47.4-62.3	23.2-53.95
			July	Source proportion (%)	**3.8 (3.0)**	**58.1 (1.8)**	**38.1 (3.2)**
				95% Confidence interval (%)	0-10.1	54.3-61.8	31.3-45.0
			August	Source proportion (%)	**5.4 (6.0)**	**40.3 (3.9)**	**54.3 (6.3)**
				95% Confidence interval (%)	0-17.6	32.3-48.2	41.2-67.3
			September	Source proportion (%)	**5.1 (6.9)**	**20.4 (6.1)**	**74.5 (4.9)**
				95% Confidence interval (%)	0-19.0	7.5-33.4	64.3-84.7
			October	Source proportion (%)	**5.8 (9.3)**	**34.2 (8.0)**	**59.9 (6.5)**
				95% Confidence interval (%)	0-25.9	15.3-53.2	44.5-75.5

	Pailugou	2700	**May**	Source proportion (%)	**1.1 (16.9)**	**21.0 (9.5)**	**78.0 (22.9)**
				95% Confidence interval (%)	0-37.3	0-42.9	27.0-100.0
			June	Source proportion (%)	**0.9 (5.9)**	**39.2 (3.9)**	**59.9 (8.7)**
				95% Confidence interval (%)	0-12.7	31.2-47.2	42.3-77.4
			July	Source proportion (%)	**0.4 (5.1)**	**49.1 (3.5)**	**50.4 (7.8)**
				95% Confidence interval (%)	0-10.8	41.9-56.4	34.4-66.4
			August	Source proportion (%)	**1.2 (8.6)**	**41.3 (5.7)**	**57.5 (12.7)**
				95% Confidence interval (%)	0-18.5	29.5-53.2	31.8-83.3
			September	Source proportion (%)	**1.0 (5.2)**	**45.0 (3.2)**	**54.0 (7.4)**
				95% Confidence interval (%)	0-11.5	38.3-51.7	38.8-69.3
			October	Source proportion (%)	**2.5 (10.7)**	**14.7 (8.9)**	**82.9 (18.0)**
				95% Confidence interval (%)	0-25.5	0-36.3	42.2-100.0
Middle reaches	Artificial oasis	1550	**May**	Source proportion (%)	**13.8 (1.3)**	**37.9 (0.6)**	**48.3 (1.3)**
				95% Confidence interval (%)	10.3-17.3	36.5-39.3	45.1-51.5
			June	Source proportion (%)	**12.1 (1.2)**	**26.6 (0.7)**	**61.3 (1.5)**
				95% Confidence interval (%)	8.9-15.2	24.8-28.4	57.8-64.9
			July	Source proportion (%)	**9.6 (1.3)**	**40.6 (0.9)**	**49.8 (2.0)**
				95% Confidence interval (%)	6.6-12.7	38.0-43.2	45.1-54.4
			August	Source proportion (%)	**8.5 (1.2)**	**39.0 (1.2)**	**52.5 (2.2)**
				95% Confidence interval (%)	5.7-11.3	36.0-42.1	47.4-57.6
			September	Source proportion (%)	**4.1 (1.0)**	**36.7 (0.6)**	**59.2 (1.3)**
				95% Confidence interval (%)	1.7-6.5	35.1-38.3	56.1-62.3
	Desert-oasis ecotone	1400	**May**	Source proportion (%)	**44.3 (4.8)**	**15.6 (2.4)**	**40.1 (2.8)**
				95% Confidence interval (%)	34.7-53.9	10.6-20.6	34.3-45.9
			June	Source proportion (%)	**44.3 (6.7)**	**6.7 (2.8)**	**48.9 (4.6)**
				95% Confidence interval (%)	30.7-58.0	0.8-12.6	39.6-58.3
			July	Source proportion (%)	**46.7 (9.2)**	**12.8 (4.4)**	**40.4 (5.5)**
				95% Confidence interval (%)	28.1-65.4	3.6-22.0	29.3-51.6
			August	Source proportion (%)	**51.2 (12.9)**	**13.2 (4.9)**	**35.6 (8.8)**
				95% Confidence interval (%)	25.2-77.3	3.2-23.3	17.6-53.6
			September	Source proportion (%)	**34.9 (9.4)**	**12.3 (6.4)**	**52.8 (3.4)**

				95% Confidence interval (%)	15.9-53.9	0-25.3	45.8-59.7
	Gobi	1400	**May**	Source proportion (%)	**(-5.7) (2.2)**	**16.7 (1.5)**	**89.1 (1.0)**
				95% Confidence interval (%)	0-(-0.8)	13.2-20.1	86.7-91.4
			June	Source proportion (%)	**15.8 (4.3)**	**13.5 (2.7)**	**70.7 (1.8)**
				95% Confidence interval (%)	7.0-24.6	7.8-19.1	66.9-74.6
			July	Source proportion (%)	**12.2 (4.6)**	**16.8 (2.9)**	**71.0 (1.9)**
				95% Confidence interval (%)	2.8-21.6	10.7-23.0	67.0-74.9
			August	Source proportion (%)	**4.9 (4.0)**	**10.0 (2.6)**	**85.1 (1.6)**
				95% Confidence interval (%)	0-13.8	4.0-15.9	81.2-89.0
			September	Source proportion (%)	**4.4 (3.6)**	**18.5 (3.1)**	**77.1 (0.8)**
				95% Confidence interval (%)	0-12.5	11.5-25.4	75.1-79.1
Lower reaches	Riparian forest	930	**May**	Source proportion (%)	**(-6.1) (16.2)**	**44.7 (10.9)**	**61.4 (25.7)**
				95% Confidence interval (%)	0-100	0-100	0-100
			June	Source proportion (%)	**(-23.9) (12.0)**	**4.6 (11.9)**	**119.3 (22.2)**
				95% Confidence interval (%)	0-100	0-100	23.8-100
			July	Source proportion (%)	**(-5.6) (8.5)**	**24.7 (12.7)**	**80.9 (20.2)**
				95% Confidence interval (%)	0-12.1	0-53	37.2-100.0
			August	Source proportion (%)	**(-14.8) (9.5)**	**12.5 (13.1)**	102.3 (21.9)
				95% Confidence interval (%)	0-7.1	0-49.0	46.0-100.0
			September	Source proportion (%)	**(-18.1) (13.1)**	**40.9 (10.5)**	**77.2 (22.5)**
				95% Confidence interval (%)	0-12.9	11.6-70.1	19.5-100.0

Table 4

Measurement uncertainty for the modeled results based on the three-component isotopic mixing model (TCIMM) and comparison with the Monte Carlo method (MCM). Contributors to precipitation: the mean transpiration fraction (f_{Tr}), evaporation fraction (f_{Ev}) and advection fraction (f_{Adv}), respectively. S.D. indicates the standard deviation.

Study regions	Sampling sites	Month	TCIMM results			MCM results (mean ± standard deviation		
			f_{Tr} (%)	f_{Ev} (%)	f_{Adv} (%)	f_{Tr} (%) ± S.D.	f_{Ev} (%) ± S.D.	f_{Adv} (%) ± S.D.
Upper Reaches	Alpine meadow at Yeniugou	From June to Aug.	**51.7**	***3.6***	44.7	**52.3 ± 5.4**	***3.5 ± 4.3***	44.2 ± 7.3
		From Sept. to Oct.	**9.9**	***6.4***	83.7	**9.5 ± 6.1**	***6.4 ± 4.0***	84.1 ± 5.5
	Alpine meadow at Hulugou	From May to Aug.	**52.4**	***5.9***	41.7	**52.7 ± 4.1**	***6.0 ± 4.3***	41.4 ± 7.5
		From Sept. to Oct.	**27.3**	***5.4***	67.3	**27.4 ± 5.5**	***5.5 ± 3.5***	67.1 ± 4.8
	Mid-mountain forest at Pailugou	From June to Sept.	**43.6**	***0.9***	55.5	**43.7 ± 5.9**	***0.2 ± 3.9***	56.1 ± 6.7
		From Sept. to Oct.	**17.6**	***1.8***	80.6	**17.7 ± 6.6**	***1.3 ± 5.7***	81.0 ± 15.1
Middle reaches	Artificial oasis at Zhangye	From May to Sept.	**36.1**	***9.5***	54.3	**35.8 ± 6.1**	***8.5 ± 3.5***	55.8 ± 12.0
	Desert-oasis ecotone at Linze	From May to Sept.	**12.2**	***44.3***	43.6	**11.9 ± 10.9**	***42.8 ± 23.2***	45.3 ± 12.9
	Gobi desert at Linze	From May to Sept.	**15.1**	***6.3***	78.6	**16.9 ± 10.6**	***2.4 ± 18.3***	80.7 ± 17.1
Lower reaches	Riparian forest in the Ejina Basin	From May to Sept.	**25.6**	***-13.5***	87.9	**23.8 ± 9.9**	***-18.7 ± 9.8***	95.0 ± 19.1

Figure captions

Fig. 1. Sampling sites and climatic data. (a) Locations of the sample sites in the Heihe River Basin. (b-f) Monthly mean air temperatures (T) and total precipitation (P) at Urumqi, Yeniugou, Pailugou, Zhangye, and Ejina. The line represents air temperature (T) and histogram represents precipitation amount (P).

Fig. 2. Seasonal variations in the $\delta^{18}O$, $\delta^{2}H$ and deuterium-excess (d-excess) in precipitation in the Heihe River Basin. Urumqi is located in the northwest of the study area. Yeniugou, Hulugou and Pailugou is located in the upper reaches (UR), and Zhangye and Ejina are located in the middle and lower reaches of the basin, respectively. Note: plot S1 was excluded from the local meteoric water line for the middle reaches.

Fig. 3. Correlations between $\delta^{18}O$ and $\delta^{2}H$ in precipitation from the alpine region (Yeniugou, Hulugou), the mid-mountain zone (Pailugou) in the upper reaches, Zhangye in the middle reaches, and Ejina in the lower reaches of the Heihe River Basin. GMWL, global meteoric water line. Note: plot S1 was excluded in the Local Meteoric Water Lines of Zhangye at the middle reaches.

Fig. 4. The effects of temperature (T) on precipitation $\delta^{18}O$ at the study sites during the raining and non-raining seasons in the Heihe River Basin. Panes (a) to (d) are based on event-precipitation data and panes (e) to (i) are based on the weighted-mean monthly precipitation.

Fig. 5. Correlations between $\delta^{18}O$ and $\delta^{2}H$ values of the shallow soil water (to a depth of 10 to 20 cm) and plant xylem water at the study sites in the Heihe River Basin. UR, upper reaches; MR, middle reaches; LR, lower reaches. GMWL, global meteoric water line; LMWL, local meteoric water line.

Fig. 6. The mean transpiration fractions (f_{Tr}), evaporation fractions (f_{Ev}) and advected fractions (f_{Adv}), and the average isotope values (in brackets, $\delta^{18}O$ and $\delta^{2}H$, respectively) for precipitation and all moisture sources, illustrating the moisture recycling characteristics. The locations are (a) Yeniugou (U-YN) from June to August, Hulugou (U-HL) from May to August, and Pailugou (U-PL) from June to September in the upper reaches; (b) Yeniugou and Hulugou from September to October, and Pailugou in May and October in the upper reaches; (c) artificial oasis (M-AO) at Zhangye, the desert-oasis ecotone (M-DO) and the Gobi (M-GB) at Linze of the

middle reaches; and (d) riparian forest in Ejina (L-EJN) from May to September in the lower reaches.

Fig. 7. Seasonal variations of the (a) transpiration fraction (f_{Tr}) and (b) evaporation fraction (f_{Ev}) in the Heihe River Basin. Value is mean ± S.D., which S.D. indicates the standard deviation. UR, upper reaches; MR, middle reaches; LR, lower reaches.

Fig. 8. Relationships between transpiration fractions derived precipitation (f_{Tr}) and (a) temperature, (b) relative humidity, (c) precipitation, and (d) vapor-pressure deficit in the Heihe River Basin (UR, upper reaches; MR, middle reaches; LR, lower reaches). Table 2 summarizes the measurement periods. In the upper reaches, we sampled alpine meadow at Yeniugou and Hulugou, and mid-mountain forest at Pailugou. In the middle reaches, we sampled the artificial oasis at Zhangye, and the desert-oasis ecotone and Gobi at Linze. In the lower reaches, we sampled the riparian forest at Ejina.

Fig. 9. Relationships between evaporation fractions derived precipitation (f_{Ev}) and (a) temperature, (b) relative humidity, and (c) vapor-pressure deficit in the Heihe River Basin (UR, upper reaches; MR, middle reaches; LR, lower reaches). Table 2 summarizes the measurement periods. In the upper reaches, we sampled alpine meadow at Yeniugou and Hulugou, and mid-mountain forest at Pailugou. In the middle reaches, we sampled the artificial oasis at Zhangye, and the desert-oasis ecotone and Gobi at Linze. In the lower reaches, we sampled the riparian forest at Ejina.

Figure 1

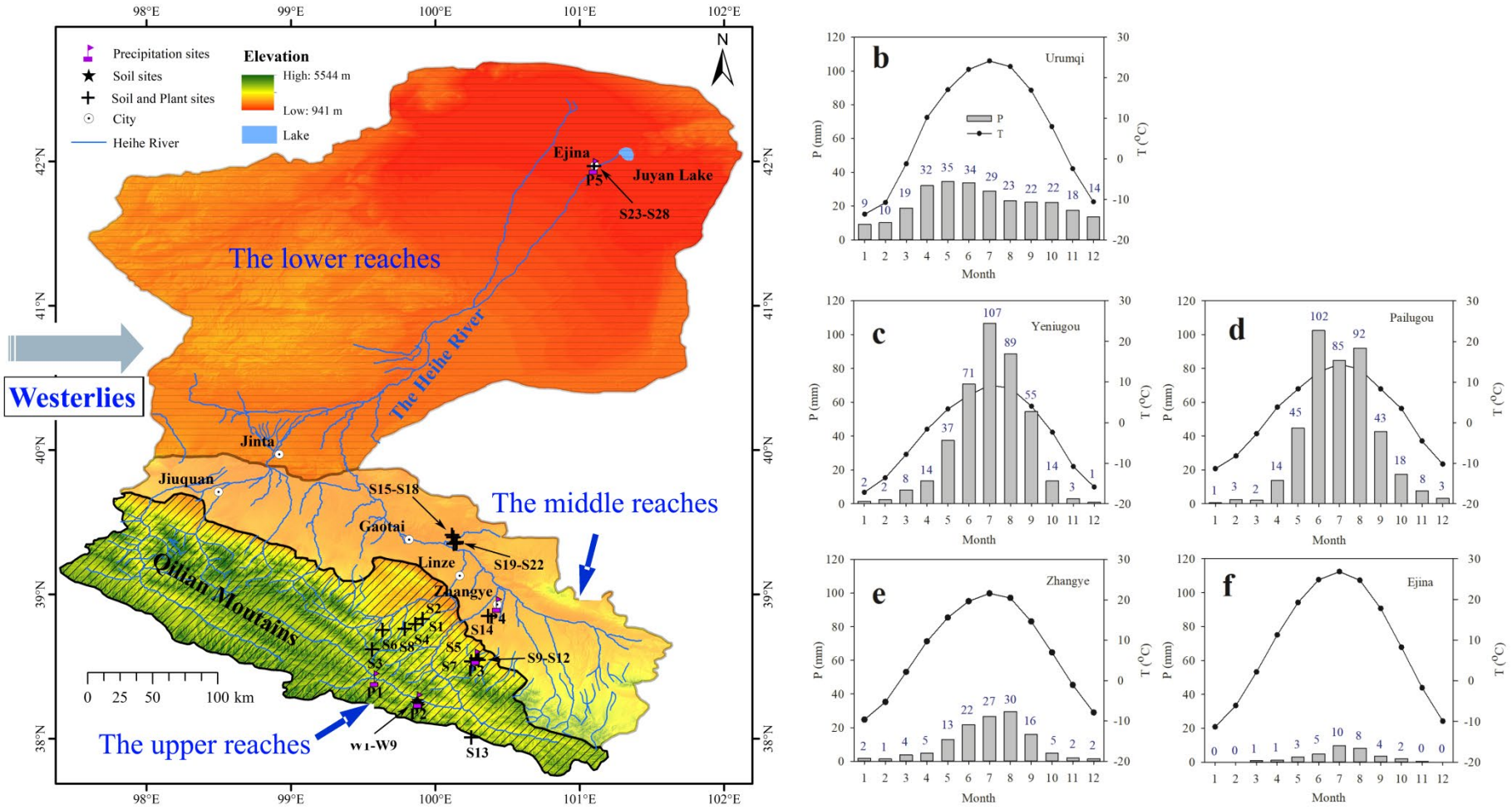
Precipitation sites
Soil sites
Soil and Plant sites
City
Heihe River
Elevation
High: 5544 m
Low: 941 m
Lake
N
Ejina
P5
Juyan Lake
S23-S28
The lower reaches
The Heihe River
Westerlies
Jinta
Jiuquan
S15-S18
The middle reaches
Gaotai
Linze
S19-S22
Zhangye
Qilian Moutains
S2
S1
S14
S4
S6
S8
S5
S7
S3
P4
P3
S9-S12
P1
P2
W1-W9
S13
The upper reaches
0 25 50 100 km
98°E
99°E
100°E
101°E
102°E
42°N
41°N
40°N
39°N
38°N
b
Urumqi
c
Yeniugou
d
Pailugou
e
Zhangye
f
Ejina
P (mm)
T (°C)
Month

Figure 2

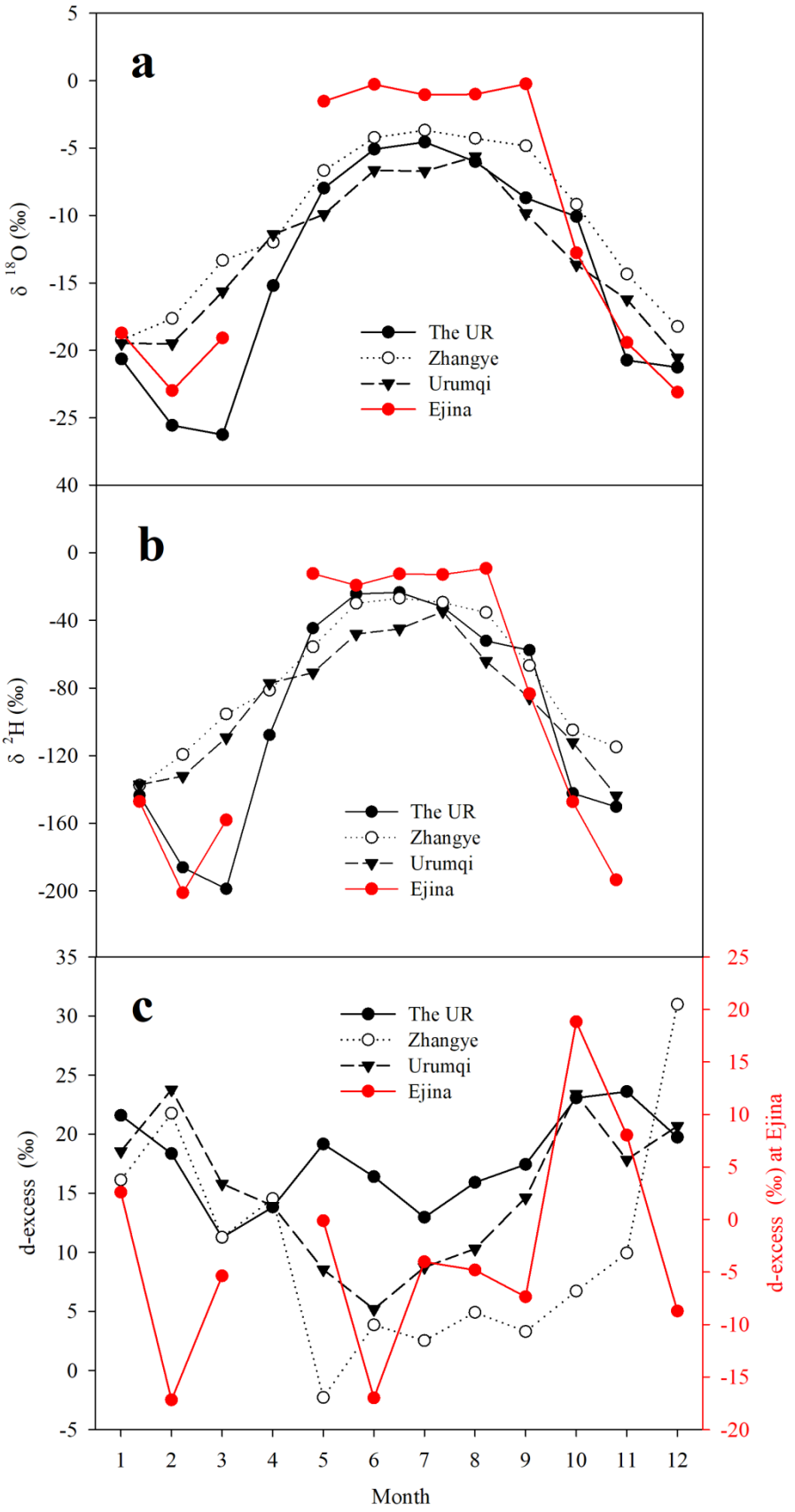
a
b
c
The UR
Zhangye
Urumqi
Ejina
δ 18O (‰)
δ 2H (‰)
d-excess (‰)
d-excess (‰) at Ejina
Month

Figure 3

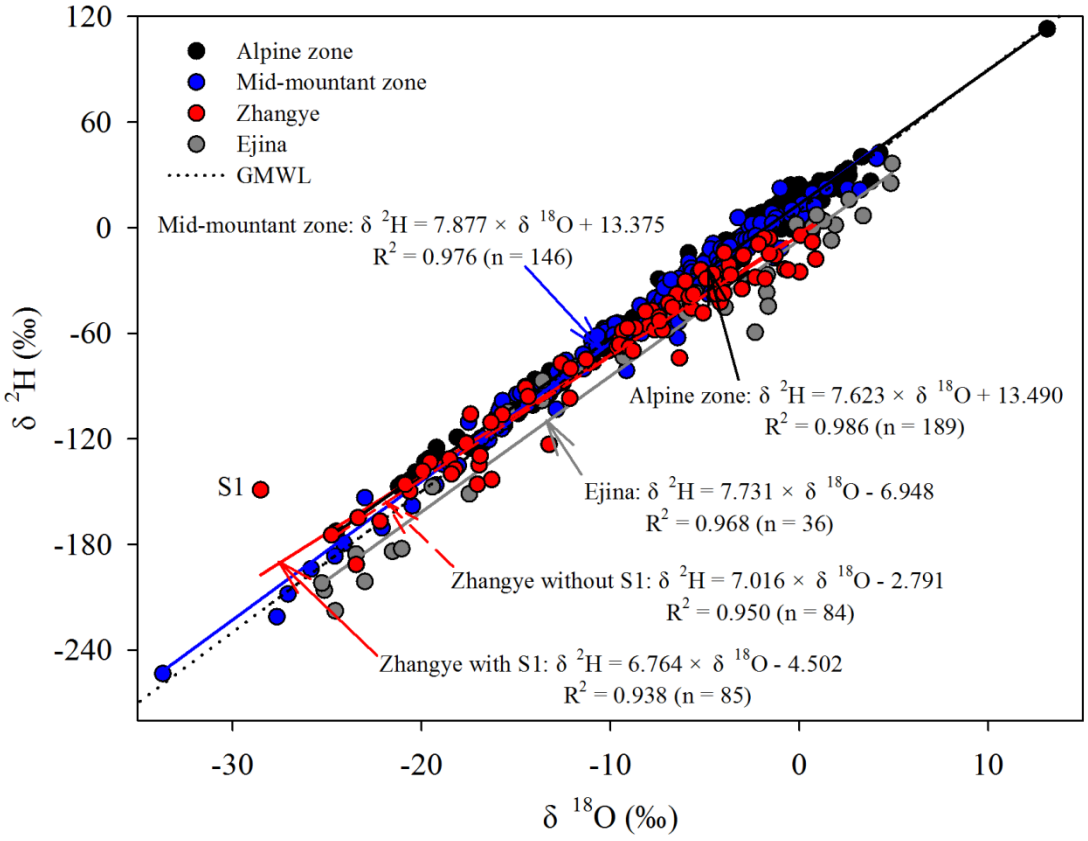
Alpine zone
Mid-mountant zone
Zhangye
Ejina
GMWL
Mid-mountant zone: δ 2H = 7.877 × δ 18O + 13.375
R2 = 0.976 (n = 146)
Alpine zone: δ 2H = 7.623 × δ 18O + 13.490
R2 = 0.986 (n = 189)
Ejina: δ 2H = 7.731 × δ 18O - 6.948
R2 = 0.968 (n = 36)
Zhangye without S1: δ 2H = 7.016 × δ 18O - 2.791
R2 = 0.950 (n = 84)
Zhangye with S1: δ 2H = 6.764 × δ 18O - 4.502
R2 = 0.938 (n = 85)
S1
120
60
0
-60
-120
-180
-240
-30
-20
-10
0
10
δ 2H (‰)
δ 18O (‰)

Figure 4

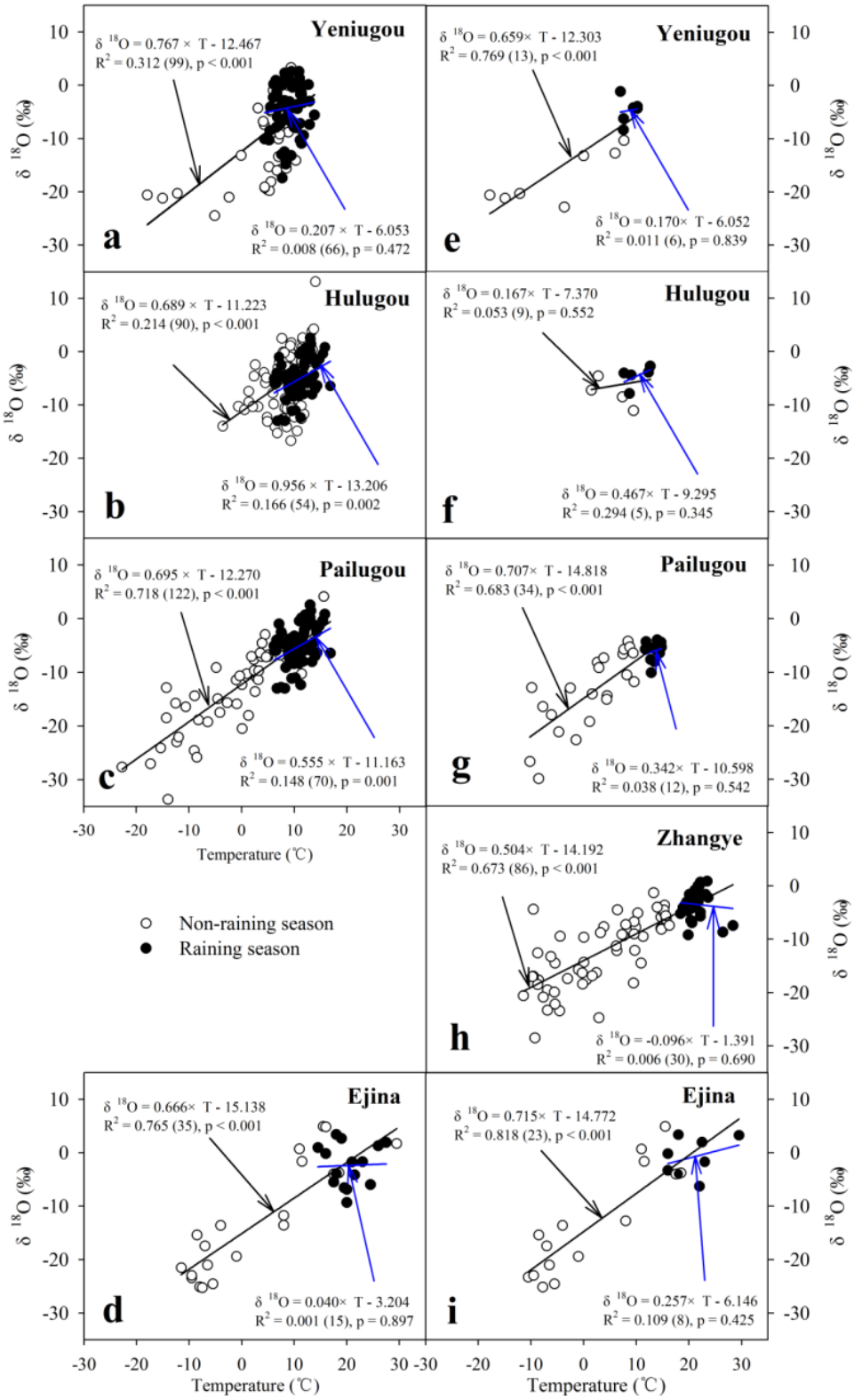
Yeniugou
δ 18O = 0.767 × T - 12.467
R2 = 0.312 (99), p < 0.001
δ 18O = 0.207 × T - 6.053
R2 = 0.008 (66), p = 0.472
a
Yeniugou
δ 18O = 0.659× T - 12.303
R2 = 0.769 (13), p < 0.001
δ 18O = 0.170× T - 6.052
R2 = 0.011 (6), p = 0.839
e
Hulugou
δ 18O = 0.689 × T - 11.223
R2 = 0.214 (90), p < 0.001
δ 18O = 0.956 × T - 13.206
R2 = 0.166 (54), p = 0.002
b
Hulugou
δ 18O = 0.167× T - 7.370
R2 = 0.053 (9), p = 0.552
δ 18O = 0.467× T - 9.295
R2 = 0.294 (5), p = 0.345
f
Pailugou
δ 18O = 0.695 × T - 12.270
R2 = 0.718 (122), p < 0.001
δ 18O = 0.555 × T - 11.163
R2 = 0.148 (70), p = 0.001
c
Pailugou
δ 18O = 0.707× T - 14.818
R2 = 0.683 (34), p < 0.001
δ 18O = 0.342× T - 10.598
R2 = 0.038 (12), p = 0.542
g
Zhangye
δ 18O = 0.504× T - 14.192
R2 = 0.673 (86), p < 0.001
δ 18O = -0.096× T - 1.391
R2 = 0.006 (30), p = 0.690
h
Ejina
δ 18O = 0.666× T - 15.138
R2 = 0.765 (35), p < 0.001
δ 18O = 0.040× T - 3.204
R2 = 0.001 (15), p = 0.897
d
Ejina
δ 18O = 0.715× T - 14.772
R2 = 0.818 (23), p < 0.001
δ 18O = 0.257× T - 6.146
R2 = 0.109 (8), p = 0.425
i
δ 18O (‰)
Temperature (℃)
Non-raining season
Raining season

Figure 5

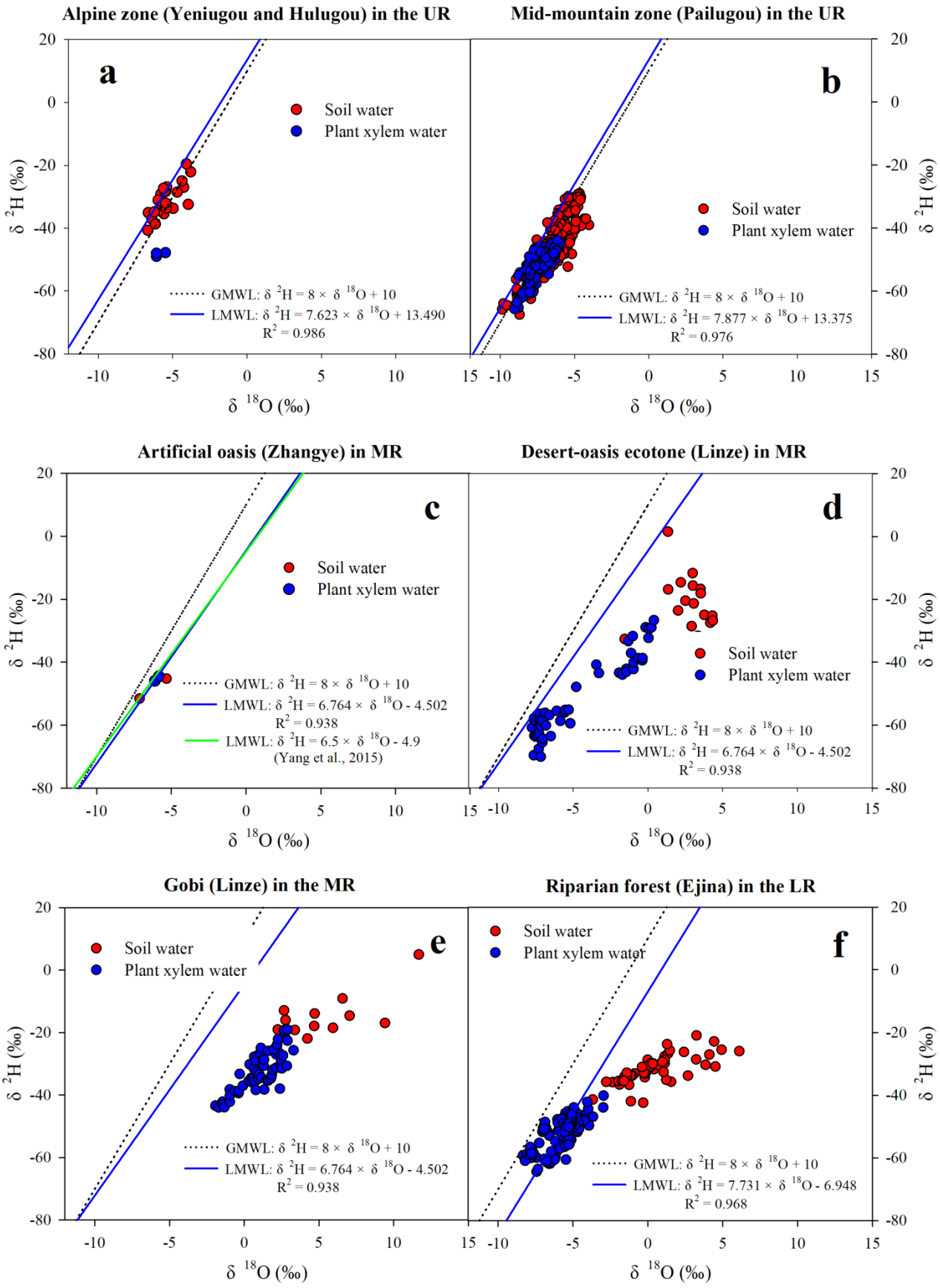
Alpine zone (Yeniugou and Hulugou) in the UR
a
Soil water
Plant xylem water
GMWL: δ 2H = 8 × δ 18O + 10
LMWL: δ 2H = 7.623 × δ 18O + 13.490
R2 = 0.986
Mid-mountain zone (Pailugou) in the UR
b
Soil water
Plant xylem water
GMWL: δ 2H = 8 × δ 18O + 10
LMWL: δ 2H = 7.877 × δ 18O + 13.375
R2 = 0.976
Artificial oasis (Zhangye) in MR
c
Soil water
Plant xylem water
GMWL: δ 2H = 8 × δ 18O + 10
LMWL: δ 2H = 6.764 × δ 18O - 4.502
R2 = 0.938
LMWL: δ 2H = 6.5 × δ 18O - 4.9
(Yang et al., 2015)
Desert-oasis ecotone (Linze) in MR
d
Soil water
Plant xylem water
GMWL: δ 2H = 8 × δ 18O + 10
LMWL: δ 2H = 6.764 × δ 18O - 4.502
R2 = 0.938
Gobi (Linze) in the MR
e
Soil water
Plant xylem water
GMWL: δ 2H = 8 × δ 18O + 10
LMWL: δ 2H = 6.764 × δ 18O - 4.502
R2 = 0.938
Riparian forest (Ejina) in the LR
f
Soil water
Plant xylem water
GMWL: δ 2H = 8 × δ 18O + 10
LMWL: δ 2H = 7.731 × δ 18O - 6.948
R2 = 0.968
δ 2H (‰)
δ 18O (‰)

Figure 6

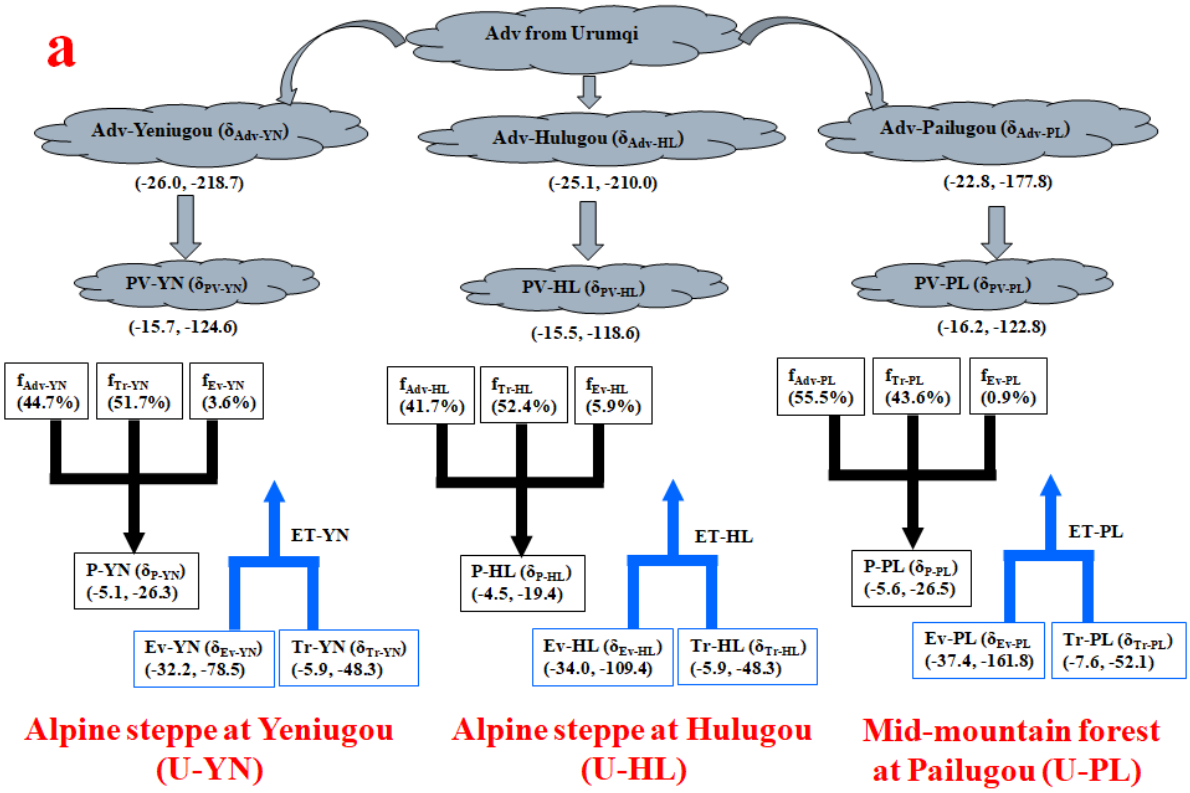
a
Adv from Urumqi
Adv-Yeniugou (δAdv-YN)
(-26.0, -218.7)
Adv-Hulugou (δAdv-HL)
(-25.1, -210.0)
Adv-Pailugou (δAdv-PL)
(-22.8, -177.8)
PV-YN (δPV-YN)
(-15.7, -124.6)
PV-HL (δPV-HL)
(-15.5, -118.6)
PV-PL (δPV-PL)
(-16.2, -122.8)
fAdv-YN (44.7%)
fTr-YN (51.7%)
fEv-YN (3.6%)
fAdv-HL (41.7%)
fTr-HL (52.4%)
fEv-HL (5.9%)
fAdv-PL (55.5%)
fTr-PL (43.6%)
fEv-PL (0.9%)
ET-YN
ET-HL
ET-PL
P-YN (δP-YN) (-5.1, -26.3)
P-HL (δP-HL) (-4.5, -19.4)
P-PL (δP-PL) (-5.6, -26.5)
Ev-YN (δEv-YN) (-32.2, -78.5)
Tr-YN (δTr-YN) (-5.9, -48.3)
Ev-HL (δEv-HL) (-34.0, -109.4)
Tr-HL (δTr-HL) (-5.9, -48.3)
Ev-PL (δEv-PL (-37.4, -161.8)
Tr-PL (δTr-PL) (-7.6, -52.1)
Alpine steppe at Yeniugou (U-YN)
Alpine steppe at Hulugou (U-HL)
Mid-mountain forest at Pailugou (U-PL)

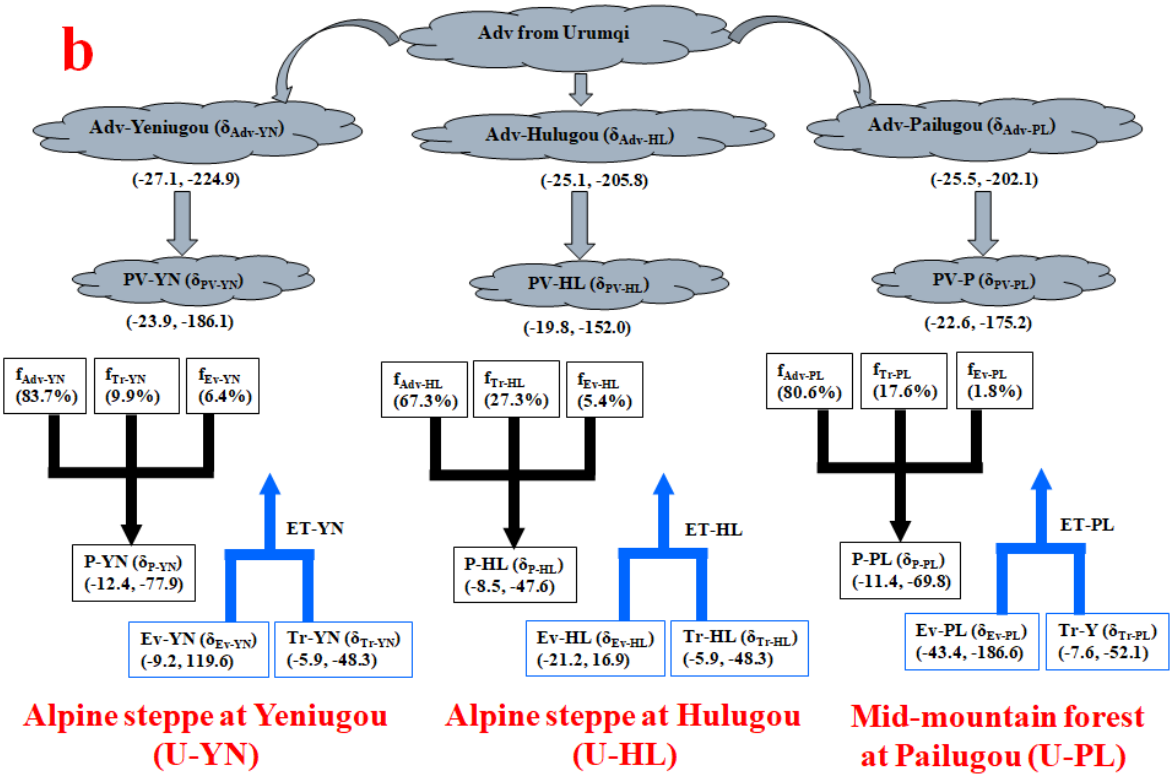
b
Adv from Urumqi
Adv-Yeniugou (δAdv-YN)
(-27.1, -224.9)
Adv-Hulugou (δAdv-HL)
(-25.1, -205.8)
Adv-Pailugou (δAdv-PL)
(-25.5, -202.1)
PV-YN (δPV-YN)
(-23.9, -186.1)
PV-HL (δPV-HL)
(-19.8, -152.0)
PV-P (δPV-PL)
(-22.6, -175.2)
fAdv-YN (83.7%)
fTr-YN (9.9%)
fEv-YN (6.4%)
fAdv-HL (67.3%)
fTr-HL (27.3%)
fEv-HL (5.4%)
fAdv-PL (80.6%)
fTr-PL (17.6%)
fEv-PL (1.8%)
ET-YN
ET-HL
ET-PL
P-YN (δP-YN) (-12.4, -77.9)
P-HL (δP-HL) (-8.5, -47.6)
P-PL (δP-PL) (-11.4, -69.8)
Ev-YN (δEv-YN) (-9.2, 119.6)
Tr-YN (δTr-YN) (-5.9, -48.3)
Ev-HL (δEv-HL) (-21.2, 16.9)
Tr-HL (δTr-HL) (-5.9, -48.3)
Ev-PL (δEv-PL) (-43.4, -186.6)
Tr-Y (δTr-PL) (-7.6, -52.1)
Alpine steppe at Yeniugou (U-YN)
Alpine steppe at Hulugou (U-HL)
Mid-mountain forest at Pailugou (U-PL)

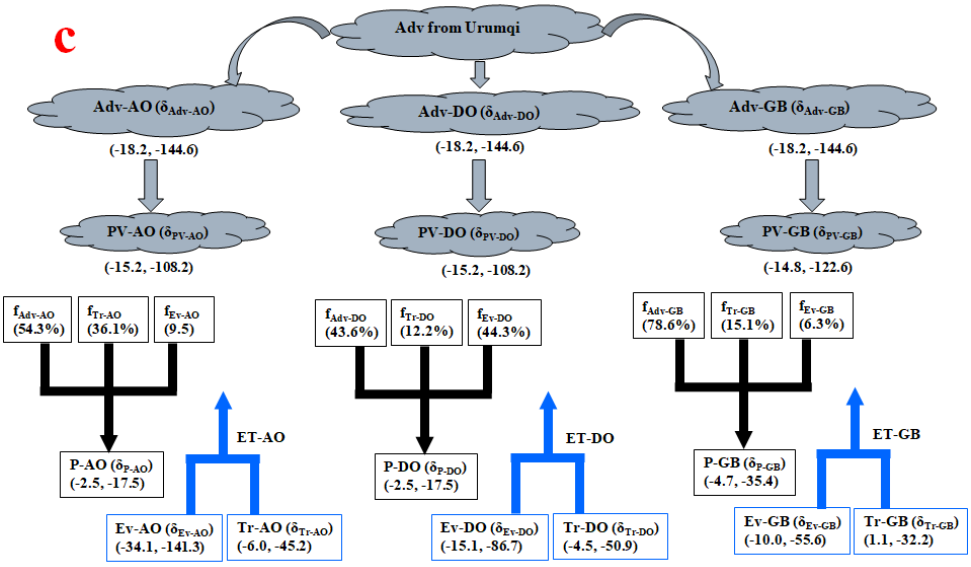

Artificial oasis (M-AO) at Zhangye

Desert-oasis ecotone (M-DO) at Zhangye

Gobi zone (M-GB) at Linze

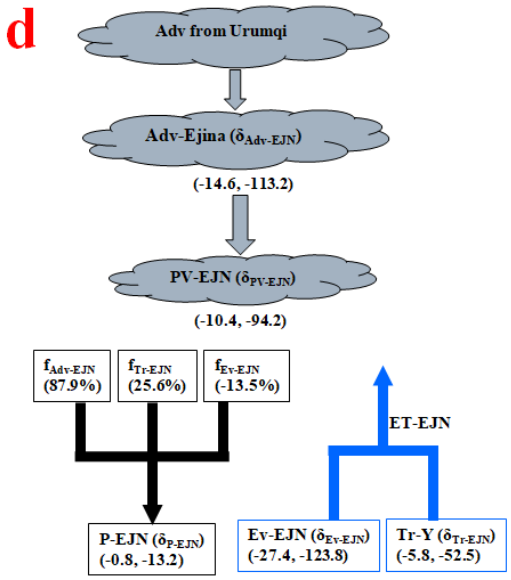

Riparian forest at Ejina (L-EJN)

Figure 7

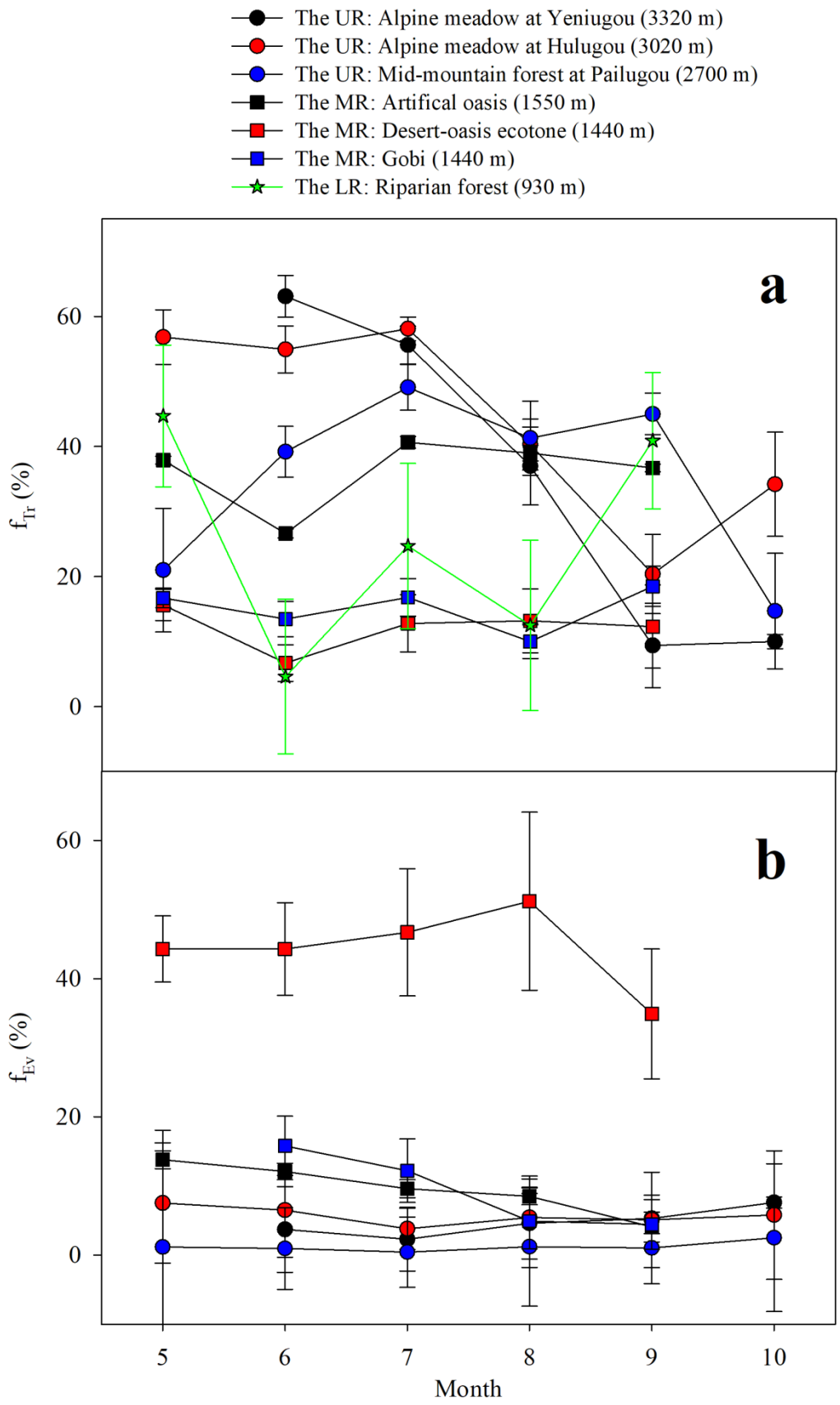
The UR: Alpine meadow at Yeniugou (3320 m)
The UR: Alpine meadow at Hulugou (3020 m)
The UR: Mid-mountain forest at Pailugou (2700 m)
The MR: Artifical oasis (1550 m)
The MR: Desert-oasis ecotone (1440 m)
The MR: Gobi (1440 m)
The LR: Riparian forest (930 m)
a
b
f_{Tr} (%)
f_{Ev} (%)
0
20
40
60
5
6
7
8
9
10
Month

Figure 8

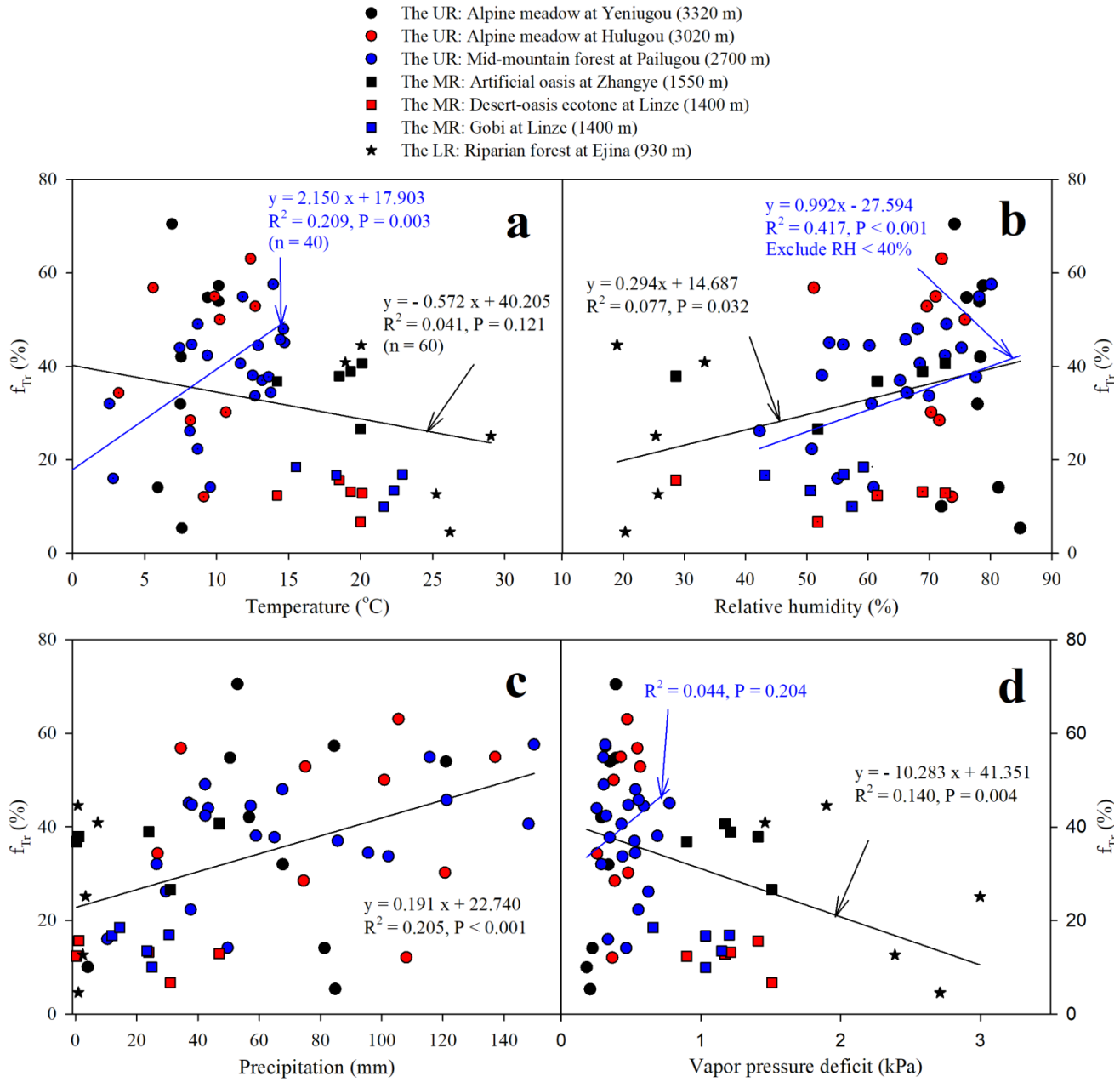
The UR: Alpine meadow at Yeniugou (3320 m)
The UR: Alpine meadow at Hulugou (3020 m)
The UR: Mid-mountain forest at Pailugou (2700 m)
The MR: Artificial oasis at Zhangye (1550 m)
The MR: Desert-oasis ecotone at Linze (1400 m)
The MR: Gobi at Linze (1400 m)
The LR: Riparian forest at Ejina (930 m)
a
y = 2.150 x + 17.903
R2 = 0.209, P = 0.003
(n = 40)
y = - 0.572 x + 40.205
R2 = 0.041, P = 0.121
(n = 60)
fTr (%)
Temperature (°C)
b
y = 0.992x - 27.594
R2 = 0.417, P < 0.001
Exclude RH < 40%
y = 0.294x + 14.687
R2 = 0.077, P = 0.032
Relative humidity (%)
c
y = 0.191 x + 22.740
R2 = 0.205, P < 0.001
Precipitation (mm)
d
R2 = 0.044, P = 0.204
y = - 10.283 x + 41.351
R2 = 0.140, P = 0.004
Vapor pressure deficit (kPa)

Figure 9

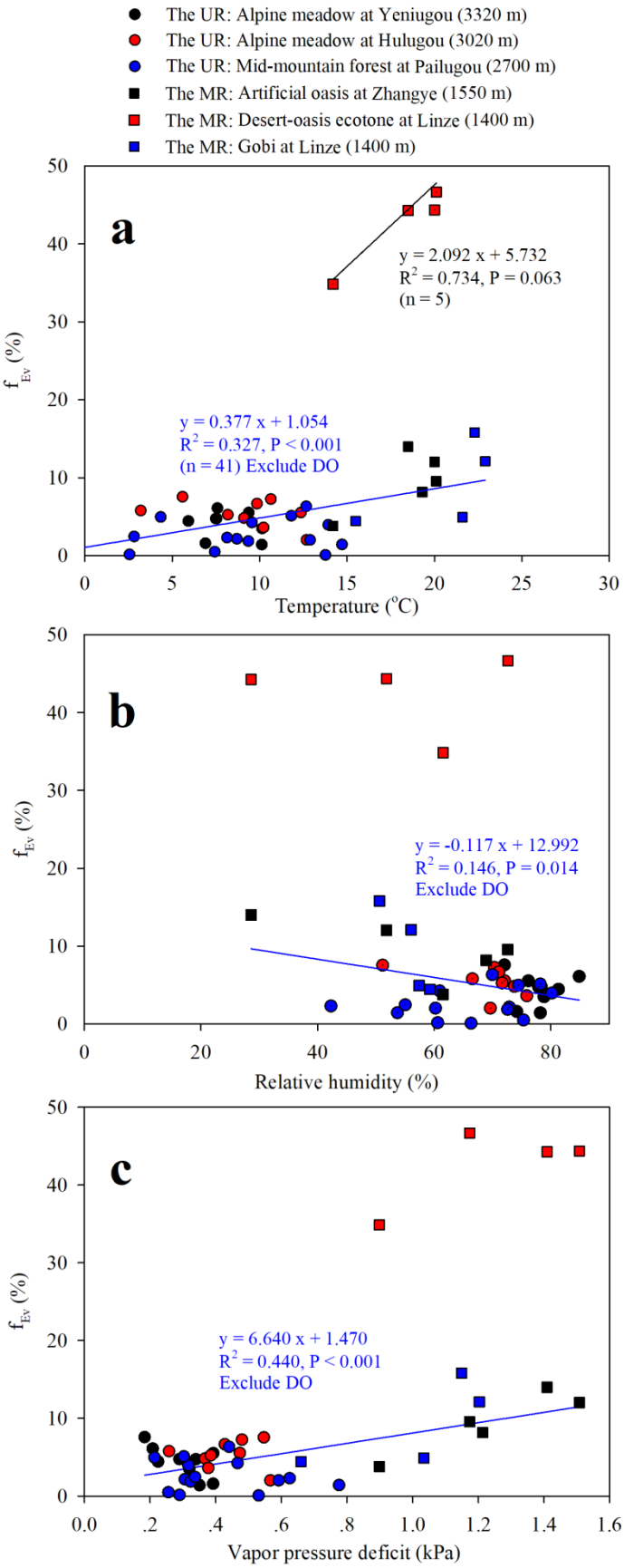
The UR: Alpine meadow at Yeniugou (3320 m)
The UR: Alpine meadow at Hulugou (3020 m)
The UR: Mid-mountain forest at Pailugou (2700 m)
The MR: Artificial oasis at Zhangye (1550 m)
The MR: Desert-oasis ecotone at Linze (1400 m)
The MR: Gobi at Linze (1400 m)
a
y = 2.092 x + 5.732
R2 = 0.734, P = 0.063
(n = 5)
y = 0.377 x + 1.054
R2 = 0.327, P < 0.001
(n = 41) Exclude DO
fEv (%)
Temperature (°C)
b
y = -0.117 x + 12.992
R2 = 0.146, P = 0.014
Exclude DO
fEv (%)
Relative humidity (%)
c
y = 6.640 x + 1.470
R2 = 0.440, P < 0.001
Exclude DO
fEv (%)
Vapor pressure deficit (kPa)

Contribution of recycled moisture to local precipitation in the inland Heihe River Basin

Liangju Zhao[a, b,*], Xiaohong Liu[c], Ninglian Wang[a], Yanlong Kong[d], Yaoxuan Song[b], Zhibin He[b], Quanyu Liu[a], Lixin Wang[e,*]

[a] Shaanxi Key Laboratory of Earth Surface System and Environmental Carrying Capacity, College of Urban and Environmental Sciences, Northwest University, Xi'an 710127, China

[b] Key Laboratory of Ecohydrology and Integrated River Basin Science, Northwest Institute of Eco-Environment and Resources, Chinese Academy of Sciences, Lanzhou 730000, China

[c] School of Geography and Tourism, Shaanxi Normal University, Xi'an 710119, China

[d] Key Laboratory of Engineering Geomechanics, Institute of Geology and Geophysics, Chinese Academy of Sciences, Beijing, China

[e] Department of Earth Sciences, Indiana University-Purdue University Indianapolis (IUPUI), Indianapolis, IN 46202, USA

Running title: Recycled moisture to precipitation

***Corresponding author**

Dr. Liangju Zhao

College of Urban and Environmental Sciences

Northwest University

Xi'an, Shann'xi, 710069, China

E-mail: zhlj@nwu.edu.cn

Cell phone：15934832330

Dr. Lixin Wang

Department of Earth Sciences

Indiana University-Purdue University Indianapolis

Indianapolis, IN, 46202, USA

E-mail: wang.iupui@gmail.com

Office phone number: 317-274-7764

Supplementary contents: tables and figures

Supplementary tables:

Table S1 List of abbreviations used for the key experimental parameters.

Table S2 Main data needed for calculation of precipitation sources and the calculated results: the moisture fractions from transpiration (f_{Tr}), evaporation (f_{Ev}), and advection (f_{Adv}) in local precipitation at Yeniugou, Hulugou, and Pailugou in the upper reaches; in artificial oases, desert-oasis ecotone, and Gobi in the middle reaches; and in riparian forest in the lower reaches of the Heihe River Basin. Variables: P, T, and RH represent precipitation, temperature, and relative humidity, respectively; $\delta^{18}O_P$ and $\delta^{2}H_P$, $\delta^{18}O_{PV}$ and $\delta^{2}H_{PV}$, $\delta^{18}O_{Tr}$ and $\delta^{2}H_{Tr}$, $\delta^{18}O_{Ev}$ and $\delta^{2}H_{Ev}$, and $\delta^{18}O_{Adv}$ and $\delta^{2}H_{Adv}$ represent the $\delta^{18}O$ and $\delta^{2}H$ values for precipitation, precipitating vapor, transpired vapor, evaporated surface moisture, and advected vapor, respectively. f_{Ev}, f_{Tr}, and f_{Adv} represent the fraction of precipitation contributed by surface evaporation, plant transpiration, and advection.

Table S3 Quantification of the uncertainty of the modeled results based on the effects of instrument precision. Diff 1 and 2 represent f_{Tr}, f_{Ev} and f_{Adv} differences between modeled with the mean $\delta^{18}O_{Tr}$ and $\delta^{2}H_{Tr}$, and with mean $\delta^{18}O_{Tr}$ - 0.2 and $\delta^{2}H_{Tr}$ - 1.0, or $\delta^{18}O_{Tr}$ + 0.2 and $\delta^{2}H_{Tr}$ + 1.0, respectively.

Table S4 Quantification of the uncertainty of the modeled results based on altering the isotopic ratio of the transpiration flux by ±1‰ for $\delta^{18}O_{Tr}$ and by ±8‰ for $\delta^{2}H_{Tr}$ (assuming constant d-excess). Diff 1 and 2 represent f_{Tr}, f_{Ev} and f_{Adv} differences between modeled with the mean $\delta^{18}O_{Tr}$ and $\delta^{2}H_{Tr}$, and with mean $\delta^{18}O_{Tr}$ - 1 and $\delta^{2}H_{Tr}$ - 8, or $\delta^{18}O_{Tr}$ + 1 and $\delta^{2}H_{Tr}$ + 8, respectively.

Supplementary figure captions:

Figure S1 Geopotential height (in geopotential meters) and wind field (in m s^{-1}) at 500 hPa for July 2009, 2011, 2012, and 2014 based on the NCEP/NCAR Reanalysis datasets (https://www.esrl.noaa.gov/psd/data/gridded/data.ncep.reanalysis.html). The red dashed frames represent the location of the study region.

Figure S2 Spatial distribution of wind trajectories at three target heights (500, 1000, and 1500 m above ground level) of sampling stations for each heavy precipitation event during the summer

in the Heihe River Basin from 2008 to 2012. The sampling sites are marked with circles. The satellite-derived land cover map was acquired from Natural Earth (http://www.naturalearthdata.com).

Supplementary tables:

Table S1 List of abbreviations used for the key experimental parameters.

Acronym	The full name	Acronym	The full name
HRB	The Heihe River Basin	$\delta^{18}O$	Oxygen isotope ratio
UR	The upper reaches of the HRB	$\delta^{2}H$	Hydrogen isotope ratio
MR	The middle reaches of the HRB	GMWL	The global meteoric water line
LR	The lower reaches of the HRB	LMWL	The local meteoric water line
U-YN	The Yeniugou of the UR	$\delta^{18}O_P/\delta^{2}H_P$	$\delta^{18}O/\delta^{2}H$ of local precipitation
U-HL	The Hulugou of the UR	$\delta^{18}O_{PV}/\delta^{2}H_{PV}$	$\delta^{18}O/\delta^{2}H$ of the precipitating vapor
U-PL	The Pailugou of the UR	$\delta^{18}O_{Tr}/\delta^{2}H_{Tr}$	$\delta^{18}O/\delta^{2}H$ of the transpiration vapor
Qilian Mt.	Qilian Mountain of the UR of the HRB	$\delta^{18}O_{Ev}/\delta^{2}H_{Ev}$	$\delta^{18}O/\delta^{2}H$ of the evaporated moisture
M-AO	The artificial oasis of the MR	$\delta^{18}O_{Adv}/\delta^{2}H_{Adv}$	$\delta^{18}O/\delta^{2}H$ of the advected vapor
M-DO	The desert-oasis ecotone of the MR	f_{Tr}	The contribution of transpiration fraction
M-GB	The Gobi of the MR	f_{Ev}	The contribution of evaporation fraction
L-EJN	The Ejina of the LR	f_{Adv}	The contribution of advected fraction

Table S2 Main data needed for calculation of precipitation sources and the calculated results: the moisture fractions from transpiration (f_{Tr}), evaporation (f_{Ev}), and advection (f_{Adv}) in local precipitation at Yeniugou, Hulugou, and Pailugou in the upper reaches; in artificial oases, desert-oasis ecotone, and Gobi in the middle reaches; and in riparian forest in the lower reaches of the Heihe River Basin. Variables: P, T, and RH represent precipitation, temperature, and relative humidity, respectively; $\delta^{18}O_P$ and δ^2H_P, $\delta^{18}O_{PV}$ and δ^2H_{PV}, $\delta^{18}O_{Tr}$ and δ^2H_{Tr}, $\delta^{18}O_{Ev}$ and δ^2H_{Ev}, and $\delta^{18}O_{Adv}$ and δ^2H_{Adv} represent the $\delta^{18}O$ and δ^2H values for precipitation, precipitating vapor, transpired vapor, evaporated surface moisture, and advected vapor, respectively. f_{Ev}, f_{Tr}, and f_{Adv} represent the fraction of precipitation contributed by surface evaporation, plant transpiration, and advection. S.D. indicates the standard deviation.

Sites and elevation(m asl)	Month		P (mm)	T (°C)	RH (%)	$\delta^{18}O_P$ (‰)	δ^2H_P (‰)	$\delta^{18}O_{PV}$ (‰)	δ^2H_{PV} (‰)	$\delta^{18}O_{Tr}$ (‰)	δ^2H_{Tr} (‰)	$\delta^{18}O_{Ev}$ (‰)	δ^2H_{Ev} (‰)	$\delta^{18}O_{Adv}$ (‰)	δ^2H_{Adv} (‰)	f_{Ev} (S.D.) (%)	f_{Tr} (S.D.) (%)	f_{Adv} (S.D.) (%)
Yeniugou																		
(Upper reaches)																		
3320			74.6	9.4	76.1	-4.2	-18.8											
	6							-13.8	-109.6	-5.9	-48.3	-36.9	-133.6	-26.3	-223.7	**3.7 (6.2)**	**63.1 (3.2)**	**33.1 (6.9)**
		95% Confidence interval (%)														0-16.4	56.6-69.7	18.8-47.5
3320			125.7	10.1	78.8	-3.9	-17.7											
	7							-15	-119.7	-5.9	-48.3	-37.2	-108.6	-25.8	-214.8	**2.3 (4.6)**	**55.6 (2.9)**	**42.1 (4.4)**
		95% Confidence interval (%)														0-11.6	49.9-61.3	33.1-51.0
3320			107.7	7.5	78.1	-7.3	-42.4											
	8							-18.4	-144.5	-5.9	-48.3	-22.6	6.8	-26	-217.6	**4.6 (6.4)**	**37.0 (6.0)**	**58.3 (4.0)**
		95% Confidence interval (%)														0-17.7	24.3-49.7	49.9-66.7
	Mean		**102.7**	**9.0**	**77.7**	**-5.1**	**-26.3**	**-15.7**	**-124.6**	**-5.9**	**-48.3**	**-32.2**	**-78.5**	**-26**	**-218.7**	**51.7**	**3.6**	**44.7**
3320			99.5	6.8	83.1	-11.5	-74.2											
	9							-22.8	-177.5	-5.9	-48.3	-3.6	184.5	-25.9	-214.4	**5.3 (3.4)**	**9.4 (6.5)**	**85.3 (3.5)**
		95% Confidence interval (%)														0-12.1	0-22.5	78.1-92.4
3320			17.4	-0.1	72	-13.2	-81.5											
	10							-25.1	-194.7	-5.9	-48.3	-14.7	54.7	-28.3	-235.4	**7.6 (0.8)**	**10.0 (1.1)**	**82.4 (0.4)**
		95% Confidence interval (%)														5.6-9.6	6.8-13.1	81.3-83.5
	Mean		**58.4**	**3.3**	**77.5**	**-12.4**	**-77.9**	**-23.9**	**-186.1**	**-5.9**	**-48.3**	**-9.2**	**119.6**	**-27.1**	**-224.9**	**9.9**	**6.4**	**83.7**
Hulugou																		
(Upper reaches)																		
3020			34.4	5.6	51.1	-4.6	-16.3											
	5							-15.9	-121	-5.9	-48.3	-35.3	-127.2	-27.8	-235.5	**7.5 (8.7)**	**56.8 (4.2)**	**35.7 (8.7)**
		95% Confidence interval (%)														0-25.0	45.0-64.0	19.0-60.0

3020	6		137.1	9.8	71.1	-4.1	-15.9	-15	-114.8	-5.9	-48.3	-33.7	-116	-24.8	-209.7	6.5 (6.8)	54.9 (3.6)	38.6 (7.2)
		95% Confidence interval (%)														0-21.0	47.4-62.3	23.2-53.95
3020	7		90.3	12.5	70.8	-3.3	-12.8	-14	-108	-5.9	-48.3	-38.4	-137.7	-24.4	-201.2	3.8 (3.0)	58.1 (1.8)	38.1 (3.2)
		95% Confidence interval (%)														0-10.1	54.3-61.8	31.3-45.0
3020	8		110.8	10.4	73.1	-6.2	-32.7	-17	-130.7	-5.9	-48.3	-28.4	-56.7	-23.6	-194.6	5.4 (6.0)	40.3 (3.9)	54.3 (6.3)
		95% Confidence interval (%)														0-17.6	32.3-48.2	41.2-67.3
	Mean		**93.1**	**9.6**	**66.5**	**-4.5**	**-21.2**	**-15.5**	**-118.6**	**-5.9**	**-48.3**	**-34.0**	**-109.4**	**-25.1**	**-210.0**	**5.9**	**52.4**	**41.7**
3020	9		91.3	8.6	72.7	-9.8	-61.2	-20.8	-161.7	-5.9	-48.3	-24.6	-11.5	-24.7	-203	5.1 (6.9)	20.4 (6.1)	74.5 (4.9)
		95% Confidence interval (%)														0-19.0	7.5-33.4	64.3-84.7
3020	10		26.8	3.2	66.5	-7.2	-33.9	-18.8	-142.2	-5.9	-48.3	-24.6	-11.5	-25.6	-208.5	5.8 (9.3)	34.2 (8.0)	59.9 (6.5)
		95% Confidence interval (%)														0-25.9	15.3-53.2	44.5-75.5
	Mean		**59.1**	**5.9**	**69.6**	**-8.5**	**-47.6**	**-19.8**	**-152**	**-5.9**	**-48.3**	**-24.6**	**-11.5**	**-25.1**	**-205.8**	**5.4**	**27.3**	**67.3**
Pailugou																		
(Upper reaches)																		
2700	6		91.6	12.4	62.8	-6.3	-35.2	-16.8	-129.2	-7.6	-52.1	-36.9	-159.8	-22.5	-179.1	1.1 (16.9)	21.0 (9.5)	78.0 (22.9)
		95% Confidence interval (%)														0-37.3	0-42.9	27.0-100.0
2700	7		93.9	14.4	67	-4.6	-19.4	-15.1	-113.6	-7.6	-52.1	-35.9	-154.6	-22.3	-173.2	0.9 (5.9)	39.2 (3.9)	59.9 (8.7)
		95% Confidence interval (%)														0-12.7	31.2-47.2	42.3-77.4
2700	8		90.5	13.1	71.8	-5.2	-23	-15.9	-118.9	-7.6	-52.1	-36.5	-158	-21.5	-166.1	0.4 (5.1)	49.1 (3.5)	50.4 (7.8)
		95% Confidence interval (%)														0-10.8	41.9-56.4	34.4-66.4
2700	9		41.5	8.5	69.2	-6.1	-28.3	-17.1	-129.4	-7.6	-52.1	-40.2	-174.6	-24.6	-192.8	1.2 (8.6)	41.3 (5.7)	57.5 (12.7)
		95% Confidence interval (%)														0-18.5	29.5-53.2	31.8-83.3
	Mean		**79.4**	**12.1**	**67.7**	**-5.6**	**-26.5**	**-16.2**	**-122.8**	**-7.6**	**-52.1**	**-37.4**	**-161.8**	**-22.8**	**-177.8**	**0.9**	**43.6**	**55.5**
2700	5		38.94	8.83	51.34	-10.9	-69	-21.9	-171.6	-7.6	-52.1	-39.8	-173	-25.5	-203.7	1.0 (5.2)	45.0 (3.2)	54.0 (7.4)
		95% Confidence interval (%)														0-11.5	38.3-51.7	38.8-69.3
2700	10		10.4	3.2	55	-11.9	-70.6	-23.4	-178.8	-7.6	-52.1	-47	-200.2	-25.5	-200.5	2.5 (10.7)	14.7 (8.9)	82.9 (18.0)
		95% Confidence interval (%)														0-25.5	0-36.3	42.2-100.0
	Mean		**24.7**	**6**	**53.2**	**-11.4**	**-69.8**	**-22.6**	**-175.2**	**-7.6**	**-52.1**	**-43.4**	**-186.6**	**-25.5**	**-202.1**	**1.8**	**17.6**	**80.6**
Artificial oases																		
(Middle reaches)																		
1550	5		13.8	18.5	28.6	3.2	25.6	-16.5	-113.2	-6	-45.2	-33.2	-131.1	-20	-161.5	13.8 (1.3)	37.9 (0.6)	48.3 (1.3)

		95% Confidence interval (%)														10.3-17.3	36.5-39.3	45.1-51.5
1550			55.7	20	51.8	-7.1	-44.7	-16.2	-114.5	-6	-45.2	-32.1	-124.9	-17.5	-142.5	**12.1 (1.2)**	**26.6 (0.7)**	**61.3 (1.5)**
	6	95% Confidence interval (%)														8.9-15.2	24.8-28.4	57.8-64.9
1550			32.8	20.1	72.6	-5.7	-35.4	-14.4	-101.3	-6	-45.2	-35	-155.6	-17.3	-136.6	**9.6 (1.3)**	**40.6 (0.9)**	**49.8 (2.0)**
	7	95% Confidence interval (%)														6.6-12.7	38.0-43.2	45.1-54.4
1550			10.6	19.3	68.9	-4.5	-31.1	-13.9	-98	-6	-45.2	-36.1	-159.6	-16.2	-127.3	**8.5 (1.2)**	**39.0 (1.2)**	**52.5 (2.2)**
	8	95% Confidence interval (%)														5.7-11.3	36.0-42.1	47.4-57.6
1550			8	14.2	61.5	1.7	-2.1	-15.2	-114.1	-6	-45.2	-34.3	-135.7	-19.6	-155.3	**4.1 (1.0)**	**36.7 (0.6)**	**59.2 (1.3)**
	9	95% Confidence interval (%)														1.7-6.5	35.1-38.3	56.1-62.3
	Mean		**24.2**	**18.4**	**56.7**	**-2.5**	**-17.5**	**-15.2**	**-108.2**	**-6**	**-45.2**	**-34.1**	**-141.3**	**-18.2**	**-144.6**	**9.5**	**36.1**	**54.3**
Desert-oasis ecotone																		
(Middle reaches)																		
1400			13.8	18.5	28.6	3.2	25.6	-16.5	-113.2	-4.5	-50.9	-17.6	-91.5	-20	-161.5	**44.3 (4.8)**	**15.6 (2.4)**	**40.1 (2.8)**
	5	95% Confidence interval (%)														34.7-53.9	10.6-20.6	34.3-45.9
1400			55.7	20	51.8	-7.1	-44.7	-16.2	-114.5	-4.5	-50.9	-16.5	-93.3	-17.5	-142.5	**44.3 (6.7)**	**6.7 (2.8)**	**48.9 (4.6)**
	6	95% Confidence interval (%)														30.7-58.0	0.8-12.6	39.6-58.3
1400			32.8	20.1	72.6	-5.7	-35.4	-14.4	-101.3	-4.5	-50.9	-14.6	-84.6	-17.3	-136.6	**46.7 (9.2)**	**12.8 (4.4)**	**40.4 (5.5)**
	7	95% Confidence interval (%)														28.1-65.4	3.6-22.0	29.3-51.6
1400			10.6	19.3	68.9	-4.5	-31.1	-13.9	-98	-4.5	-50.9	-14.6	-89.9	-16.2	-127.3	**51.2 (12.9)**	**13.2 (4.9)**	**35.6 (8.8)**
	8	95% Confidence interval (%)														25.2-77.3	3.2-23.3	17.6-53.6
1400			8	14.2	61.5	1.7	-2.1	-15.2	-114.1	-4.5	-50.9	-12.2	-74.1	-19.6	-155.3	**34.9 (9.4)**	**12.3 (6.4)**	**52.8 (3.4)**
	9	95% Confidence interval (%)														15.9-53.9	0-25.3	45.8-59.7
	Mean		**24.2**	**18.4**	**56.7**	**-2.5**	**-17.5**	**-15.2**	**-108.2**	**-4.5**	**-50.9**	**-15.1**	**-86.7**	**-18.2**	**-144.6**	**44.3**	**12.2**	**43.6**
Gobi																		
(Middle reaches)																		
1400			11.9	16.1	43.4	-6.7	-55.6	-16.9	-145.9	1.1	-32.2	-13.1	-56.8	-20	-161.5	**(-5.7) (2.2)**	**16.7 (1.5)**	**89.1 (1.0)**
	5	95% Confidence interval (%)														0-(-0.8)	13.2-20.1	86.7-91.4
1400			23.3	20.1	51.3	-4.2	-29.9	-14.1	-115.3	1.1	-32.2	-11.8	-64.8	-17.5	-142.5	**15.8 (4.3)**	**13.5 (2.7)**	**70.7 (1.8)**
	6	95% Confidence interval (%)														7.0-24.6	7.8-19.1	66.9-74.6
1400			30.5	22.2	55.2	-3.7	-26.9	-13.4	-109.9	1.1	-32.2	-10.5	-61.6	-17.3	-136.6	**12.2 (4.6)**	**16.8 (2.9)**	**71.0 (1.9)**
	7	95% Confidence interval (%)														2.8-21.6	10.7-23.0	67.0-74.9

1400			24.9	20.6	57.3	-4.3	-29.3	-14.1	-114.3	1.1	-32.2	-8.7	-55.1	-16.2	-127.3	**4.9 (4.0)**	**10.0 (2.6)**	**85.1 (1.6)**
	8	95% Confidence interval (%)														0-13.8	4.0-15.9	81.2-89.0
1400			14.4	14.7	60.7	-4.8	-35.3	-15.2	-127.4	1.1	-32.2	-6	-39.5	-19.6	-155.3	**4.4 (3.6)**	**18.5 (3.1)**	**77.1 (0.8)**
	9	95% Confidence interval (%)														0-12.5	11.5-25.4	75.1-79.1
	Mean		**21**	**18.7**	**53.6**	**-4.7**	**-35.4**	**-14.8**	**-122.6**	**1.1**	**-32.2**	**-10**	**-55.6**	**-18.2**	**-144.6**	**6.3**	**15.1**	**78.6**
Riparian forest																		
(Lower reaches)																		
930			0.8	20	19	-1.5	-12.3	-11.3	-97.6	-5.8	-52.5	-27.5	-124.3	-17	-132.9	**(-6.1) (16.2)**	**44.7 (10.9)**	**61.4 (25.7)**
	5	95% Confidence interval (%)														0-100	0-100	0-100
930			0.9	26.2	20.3	-0.3	-19.2	-9.6	-97.5	-5.8	-52.5	-27.5	-120.5	-13.3	-103.8	**(-23.9) (12.0)**	**4.6 (11.9)**	**119.3 (22.2)**
	6	95% Confidence interval (%)														0-100	0-100	23.8-100
930			3.3	29	25.3	-1.1	-12.4	-10.1	-87.8	-5.8	-52.5	-27.1	-122.3	-12.6	-101	**(-5.6) (8.5)**	**24.7 (12.7)**	**80.9 (20.2)**
	7	95% Confidence interval (%)														0-12.1	0-53	37.2-100.0
930			2.4	25.2	25.7	-1	-12.9	-10.4	-92.3	-5.8	-52.5	-27.2	-123.5	-13.4	-101.7	**(-14.8) (9.5)**	**12.5 (13.1)**	102.3 (21.9)
	8	95% Confidence interval (%)														0-7.1	0-49.0	46.0-100.0
930			7.3	18.9	33.3	-0.2	-9.3	-10.2	-96	-5.8	-52.5	-27.6	-128.4	-16.6	-126.6	**(-18.1) (13.1)**	**40.9 (10.5)**	**77.2 (22.5)**
	9	95% Confidence interval (%)														0-12.9	11.6-70.1	19.5-100.0
	Mean		**2.9**	**23.9**	**24.7**	**-0.8**	**-13.2**	**-10.3**	**-94.2**	**-5.8**	**-52.5**	**-27.4**	**-123.8**	**-14.6**	**-113.2**	**-13.5**	**25.6**	**87.9**

Table S3 Quantification of the uncertainty of the modeled results based on the effects of instrument precision. Diff 1 and 2 represent f_{Tr}, f_{Ev} and f_{Adv} differences between modeled with the mean $\delta^{18}O_{Tr}$ and $\delta^{2}H_{Tr}$, and with mean $\delta^{18}O_{Tr}$ - 0.2 and $\delta^{2}H_{Tr}$ - 1.0, or $\delta^{18}O_{Tr}$ + 0.2 and $\delta^{2}H_{Tr}$ + 1.0, respectively.

Pailugou	$\delta^{18}O_{Tr\text{-}Mean}$ (‰)	$\delta^{2}H_{Tr\text{-}Mean}$ (‰)		$\delta^{18}O_{Tr\text{-}Mean}$ -0.2 (‰)	$\delta^{2}H_{Tr\text{-}Mean}$ - 1 (‰)			$\delta^{18}O_{Tr\text{-}Mean}$ + 0.2 (‰)	$\delta^{2}H_{Tr\text{-}Mean}$ + 1 (‰)	
	-7.6	-52.1		-7.8	-53.1			-7.4	-51.1	
	f_{Tr}	f_{Ev}	f_{Adv}	f_{Tr}	f_{Ev}	f_{Adv}		f_{Tr}	f_{Ev}	f_{Adv}
June	39.2	0.9	59.9	39.5	0.7	59.8	June	38.8	1.1	60.1
July	49.1	0.4	50.5	49.6	0.0	50.4	July	48.7	0.5	50.8
August	41.0	1.2	57.8	41.7	0.8	57.5	August	41.0	1.2	57.9
September	45.0	1.0	54.0	45.3	0.7	54.0	September	44.6	1.1	54.3
Mean	43.6	0.9	55.5	44.0	0.5	55.4		43.3	1.0	55.8
			Diff 1	**0.4**	**-0.4**	**-0.1**	Diff 2	**-0.3**	**0.1**	**0.3**

Table S4 Quantification of the uncertainty of the modeled results based on altering the isotopic ratio of the transpiration flux by ±1‰ for $\delta^{18}O_{Tr}$ and by ±8‰ for $\delta^{2}H_{Tr}$ (assuming constant d-excess). Diff 1 and 2 represent f_{Tr}, f_{Ev} and f_{Adv} differences between modeled with the mean $\delta^{18}O_{Tr}$ and $\delta^{2}H_{Tr}$, and with mean $\delta^{18}O_{Tr}$ - 1 and $\delta^{2}H_{Tr}$ - 8, or $\delta^{18}O_{Tr}$ + 1 and $\delta^{2}H_{Tr}$ + 8, respectively.

Pailugou	$\delta^{18}O_{Tr\text{-}Mean}$ (‰)	$\delta^{2}H_{Tr\text{-}Mean}$ (‰)			$\delta^{18}O_{Tr\text{-}Mean}$ -1 (‰)	$\delta^{2}H_{Tr\text{-}Mean}$ - 8 (‰)			$\delta^{18}O_{Tr\text{-}Mean}$ + 1 (‰)	$\delta^{2}H_{Tr\text{-}Mean}$ + 8 (‰)	
	-7.6	-52.1			-8.6	-60.1			-6.6	-44.1	
	f_{Tr}	f_{Ev}	f_{Adv}		f_{Tr}	f_{Ev}	f_{Adv}		f_{Tr}	f_{Ev}	f_{Adv}
June	39.2	0.9	59.9	June	41.8	0.8	57.4	June	36.8	1.1	62.1
July	49.1	0.4	50.5	July	52.7	0.1	47.2	July	46.1	0.3	53.6
August	41.0	1.2	57.8	August	44.5	0.9	54.6	August	38.6	1.0	60.4
September	45.0	1.0	54.0	September	47.7	0.8	51.5	September	42.5	1.0	56.5
Mean	43.6	0.9	55.5		46.7	0.7	52.7		41.0	0.8	58.1
				Diff 1	**3.1**	**-0.2**	**-2.8**	Diff 2	**-2.6**	**-0.1**	**2.6**

Supplementary Figures:

Figure S1

Geopotential height (in geopotential meters) and wind field (in m s^{-1}) at 500 hPa for July 2009, 2011, 2012, and 2014 based on the NCEP/NCAR Reanalysis datasets (https://www.esrl.noaa.gov/psd/data/gridded/data.ncep.reanalysis.html). The red dashed frames represent the location of the study region.

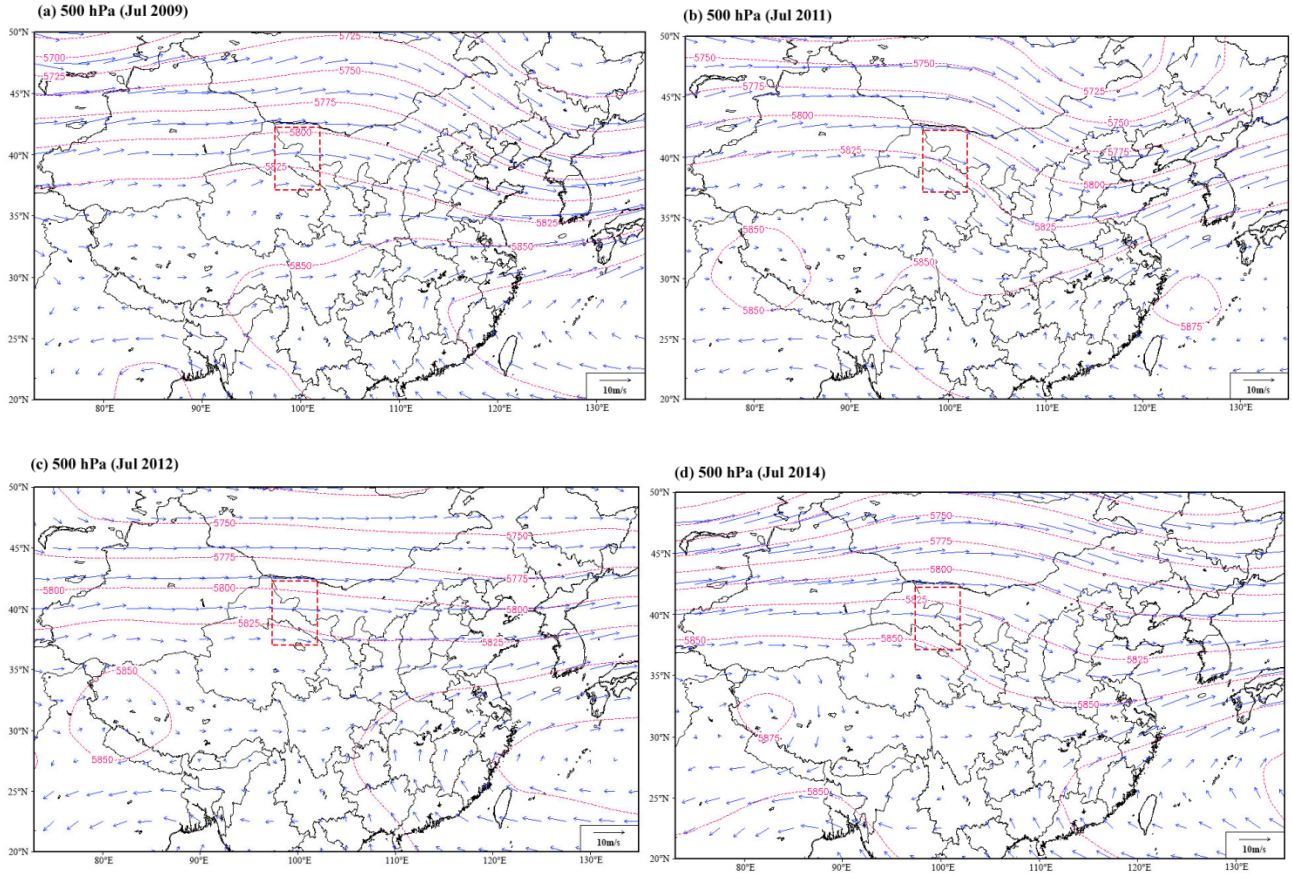

Figure S2

Spatial distribution of wind trajectories at three target heights (500, 1000, and 1500 m above ground level) of sampling stations for each heavy precipitation event during the summer in the Heihe River Basin from 2008 to 2012. The sampling sites are marked with circles. The satellite-derived land cover map was acquired from Natural Earth (http://www.naturalearthdata.com).

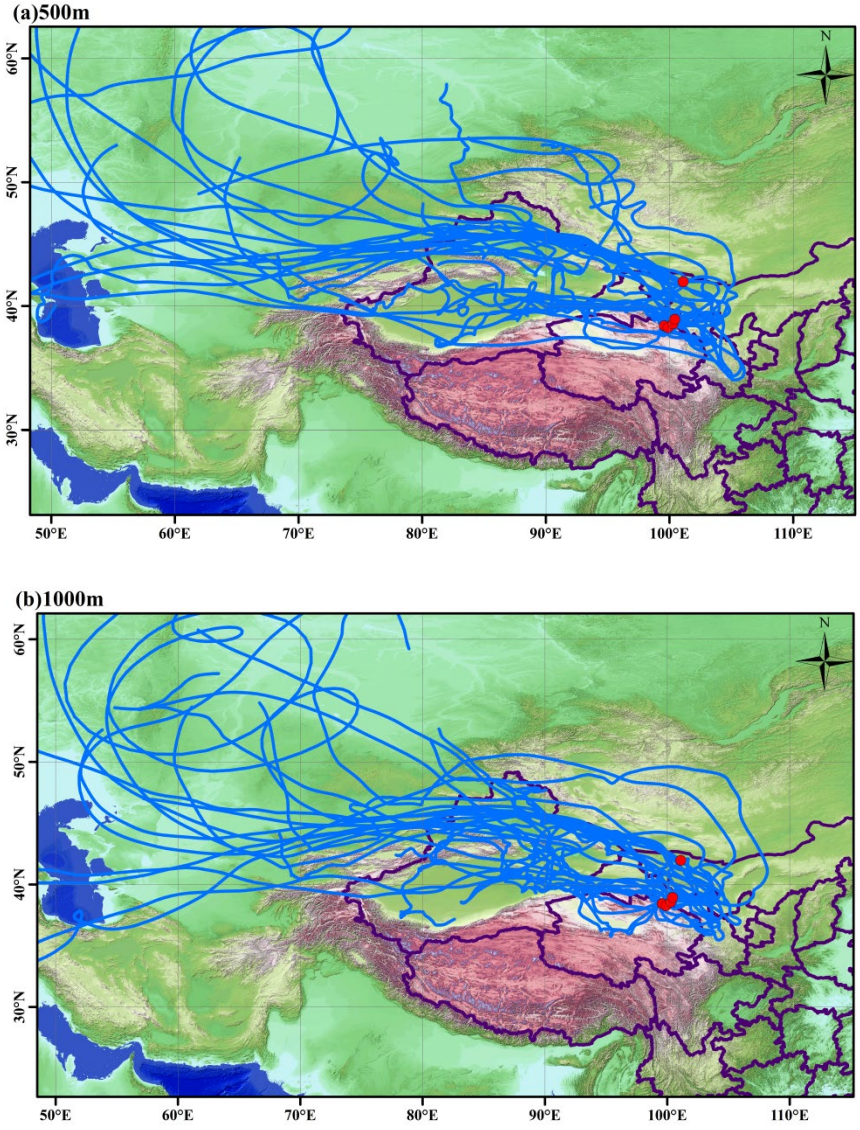

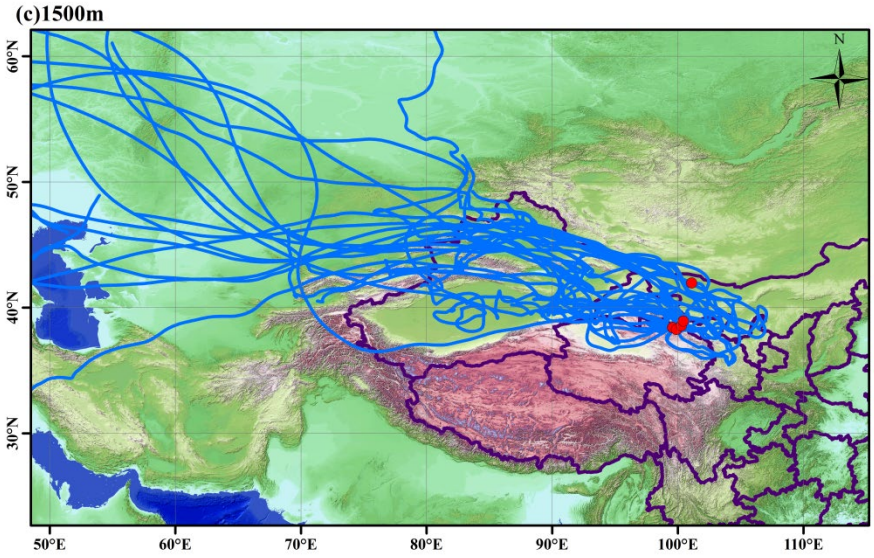
(c)1500m
60°N
50°N
40°N
30°N
50°E
60°E
70°E
80°E
90°E
100°E
110°E
N